Extracting Long-term Periodicity in Markarian 501 from Optical Wavelength Filters

McKay Douglas Osborne

A senior thesis submitted to the faculty of
Brigham Young University
in partial fulfillment of the requirements for the degree of

Bachelor of Science

J. Ward Moody, Advisor

Department of Physics and Astronomy

Brigham Young University

May 2017

Copyright © 2017 McKay Douglas Osborne

All Rights Reserved

ABSTRACT

Extracting Long-term Periodicity in Markarian 501 from Optical Wavelength Filters

McKay Douglas Osborne
Department of Physics and Astronomy, BYU
Bachelor of Science

Blazars are believed to be supermassive black holes in galactic nuclei, emitting high-energy radiation. Despite much theoretical and observational research performed on these enormous masses, the mysteries of their inner dynamics remain unsolved. BYU-owned telescopes (ROVOR and WMO) have monitored the prototypical blazar, Mrk 501, from 2009–2016 at optical wavelengths, searching for any obvious periodicity to its variations in brightness. We performed differential photometry on this data set using *Mira* and *VPhot*. The photometric calibration of these data is used to construct a low-noise light curve. Frequency analysis is performed using *Period04*. The light curve analysis unveils an obvious long-term periodicity of $\sim$2300 days. Further frequency analysis shows other possible simultaneous periods of lesser duration. These results match expectations for a multibody black hole system.

Keywords: Markarian 501, blazar, differential photometry, *Mira*, ROVOR

ACKNOWLEDGMENTS

I would like to thank my advisor, Dr. J. Ward Moody, for his guidance and patience in assisting me in the research process. He has always been there to mentor me and helped me through the learning process of becoming a better researcher. I would like to thank Joe Rivest (who worked with me) for teaching me how to use *VPhot* and helping me understand concepts (from astronomy) to perform research. I am grateful for The Department of Physics and Astronomy for allowing me research credit hours and funding that enabled me to write this thesis. I am most grateful for my beautiful wife and eternal companion, Katie, for her love, support, and encouragement as I spent many hours at school and home working on this lengthy project. I also thank my other family members and friends for their support and encouragement throughout this research process.

Contents

List of Figures

List of Tables

Chapter 1

Introduction

Markarian 501 (Mrk 501) has been monitored for the past seven years using BYU-owned telescopes, Remote Observatory for Variable Object Research (ROVOR) and West Mountain Observatory (WMO). I used the program, *Mira*, to perform differential photometry on the ROVOR data. Joseph Rivest (hereafter, Joe), another undergraduate student, performed photometry on the WMO data (Rivest Brigham Young University, Provo, U.T., 2017). I used the ROVOR and WMO data to construct a light curve. Joe and I determined a long-term period in the light curve, along with shorter periods, using *Period04*. The goal of this thesis is to demonstrate how archived data from variable objects, e.g., blazars, can be used to create a low-noise light curve and analyzed to find periodicity in brightness variations of that object. This chapter explains the foundation of my thesis: I give background information explaining what a blazar is, discuss why we chose to observe Mrk 501, present a possible theory for a binary black hole, review other research done on Mrk 501, and describe preliminary work done on Mrk 501 at BYU.

1.1 Markarian 501

Markarian 501 (Mrk 501) is a galaxy located at J2000.0 right ascension (RA) = $16^h\ 53^m\ 52.21^s$ and declination (DEC) = $39°\ 45'$ (arc min) 37.6" (arc sec), in the constellation of Hercules. Mrk 501 was the second extragalactic TeV (10^{12} eV) source to be discovered after Mrk 421 (Acciari et al. 2011). The name, Mrk 501, can refer to both the galaxy and the Active Galactic Nucleus (AGN) at its core. An AGN is a supermassive black hole (SMBH) that is absorbing mass with two bipolar jets emerging from it. To avoid confusion, the Mrk 501 that I refer to throughout this thesis corresponds to the latter.

These massive AGNs are located in the center of galaxies. They are energetic, unresolved point sources that appear brighter than their surrounding outer galactic regions. A full energy spectrum is emitted from AGNs with wavelengths spanning the whole electromagnetic spectrum. This range of emitted energies is thought to result from matter accumulating on the SMBH accretion disk.

The strong gravitational force of the SMBH attracts masses that come into its sphere of influence. As captured mass is added to the accretion disk of the black hole, the released energy effects an increase of the AGN's luminosity (Lynden-Bell 1969). As mass migrates to the interior of the disk, it is heated and ejected from the disk's magnetic poles as depicted in Figure 1.1(a). The accretion disk is represented by a dark gray ellipse having angular velocity in the $\pm\hat{\phi}$ direction (with the disk rotating into or out of the page). The two light blue cones represent the jets from the AGN. Jets are shown protruding from the accretion disk in opposite directions ($\pm\hat{z}$) at the magnetic dipoles. The event horizon is depicted as a black circle around the center of the black hole.

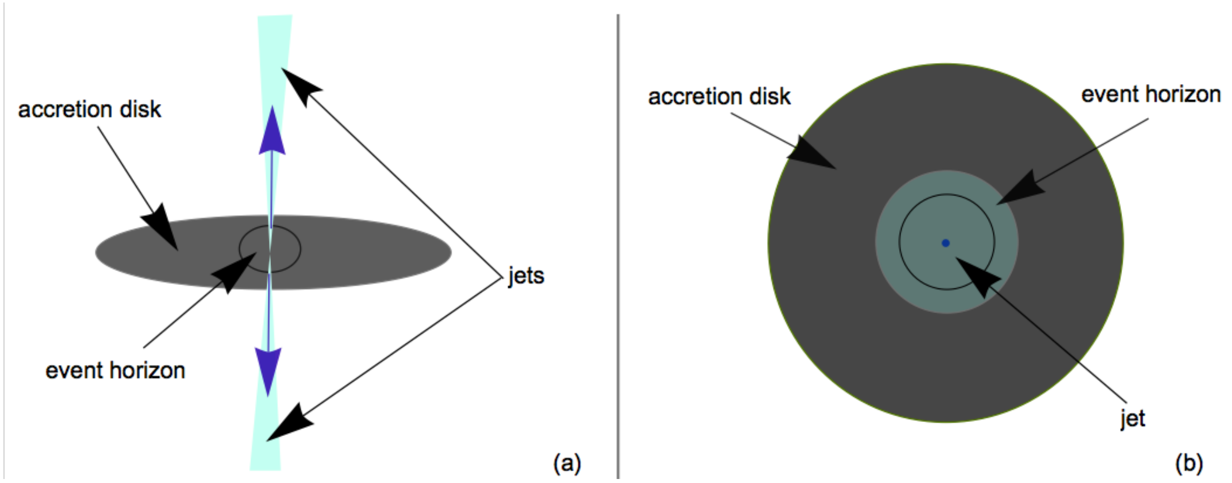

Figure 1.1 (a) Orientation of an AGN. The event horizon, accretion disk, and jets are labeled. Blue arrows show the direction of the jets' emission ($\pm\hat{z}$). The jets (light blue cones) emerge perpendicularly out from the center of the accretion disk (dark gray ellipse) plane. The event horizon is represented by the black circle surrounding the center of the black hole. The accretion disk rotates in or out of the page ($\pm\hat{\phi}$). (b) A different perspective of the AGN, with one jet directed toward Earth (along Earth's line of sight). The dark blue dot in the middle represents the direction of the jet pointing out of the page, the other jet cannot be seen. The conical geometry of the jet is implied, with the circular cross section extending from the center, shown as turquoise circle. The accretion disk in this diagram is rotating in the $\pm\hat{\theta}$ direction, around the accretion disk plane on the page. Blazar jets have a maximum tilt from Earth's line of sight of $\leq 20°$.

Mrk 501 is a specific type of AGN called a blazar. A blazar is a class of AGN in which the relativistic jet emerging from the black hole is $\leq 20°$ from Earth's line of sight (Urry & Padovani 1995) as shown in Figure 1.1(b). When blazars are observed from Earth, the observer is looking right down the barrel of the jet. The AGN is rotating around the page in the $\pm\hat{\theta}$ direction (with the disk rotating clockwise or counterclockwise on the page). The jet contains the highest energies emitted from the blazar, making it worthy of observation.

1.2 Interest in Markarian 501

According to Catanese et al. (1997), prior to 1997, Mrk 501 was not as bright as Mrk 421 (a nearby blazar). In April 1997, the observed U-band flux of Mrk 501 was 10% higher than the previous month. Mrk 501's average magnitude was found to be ∼100 times that of Mrk 421 in April 1997, making it the most energetic source in the sky, with energies in the TeV range (Catanese et al. 1997).

To be clear magnitude refers to the logarithmic scale luminosity of a given astronomical object [Eq. (1.1)]. Magnitude usually refers to the apparent magnitude of the object with smaller values are brighter values.

$$\mathrm{Mag} = 2.5 \times \log_{10}|\mathrm{N_{counts}}| \tag{1.1}$$

The number of flux counts (or luminosity) is represented by $\mathrm{N_{counts}}$. Following this famous high-energy outburst in 1997, Mrk 501 became a major target for studying high-energy physics in the TeV stage. Because the jet coming from the blazar is aimed at Earth, sending high-energy particles toward us, data taken on Mrk 501 helps verify or modify theories for galactic energy transportation and cosmic ray generation. These data could especially shed light on the SMBH theory and the conditions existing around the accretion disk.

The majority of published observations on Mrk 501 have been done while flaring, i.e., when it peaks in the magnitude. We decided to monitor Mrk 501 in what we thought would be a quiescent state to see how it normally behaves. Without understanding the normal behavior of Mrk 501, it is difficult to understand its abnormal behavior. In particular, we sought to know if there were regular brightness variations during in its non-flaring, quiescent state.

A reason for suspecting variability in the quiescent state is the possibility that Mrk 501 contains a multibody black hole system (MBHS), in which black holes orbit around the collective center of mass. Galaxy formation theory predicts such multiple systems. For example, a single sinusoidal variation in brightness supports a binary black hole model. The periodic brightening and dimming could be from the other SMBH perturbing the first SMBH and its accretion disk changing the apparent magnitude in a sinusoidal manner. A more detailed explanation for how Mrk 501 gives evidence for a binary black hole system can be found in Rivest (2017, Brigham Young University).

1.3 Previous Work from Literature

Blazar variability can be broken into three kinds: intra-day/intra-night (minutes to hours), short-term (weeks to months), and long-term (months to years). Gupta et al. (2008) observed Mrk 501 in Johnson B, V, and R filters, finding intra-night variation in R of 0.5 mag in 15 min. Because I will be referring to the B, V, R, and I filters throughout this thesis, I have included a plot from astrodon.com (Figure 1.2), illustrating transmitted wavelength values through each filter. Later Gupta et al. (2012) determined the black hole mass to be 3.72×10^7 $M_\odot$ from observed optical data. Barbieri & Romano et al. (1977) found long-term variations of 0.9 mag at optical wavelengths after observing Mrk 501 for a few years. Minute-long, fast variations were reported in the 2014 gamma ray flare by Chakrabotry et al. (2015). Variations in radio wavelengths are yet to be reported (Kondo et al. 1981).

Acciari et al. (2011) studied differences between the March 2009 and 1997 flares. Four different telescopes monitored Mrk 501 over a few nights in ranges from x-ray to very high-energy (VHE), i.e., energy above 100 GeV (0.1 TeV). They found that during this period, Mrk 501 had an x-ray flare with one order of magnitude higher than in 1997, however the VHE data remained relatively stable. They concluded that more observations are needed to understand variations at multiple wavelengths (Acciari et al. 2011).

Cologna et al. (2015) conducted a campaign involving multiple telescopes capable of observing high-energy, x-ray, and optical wavelengths. Flaring states were found at both x-ray and

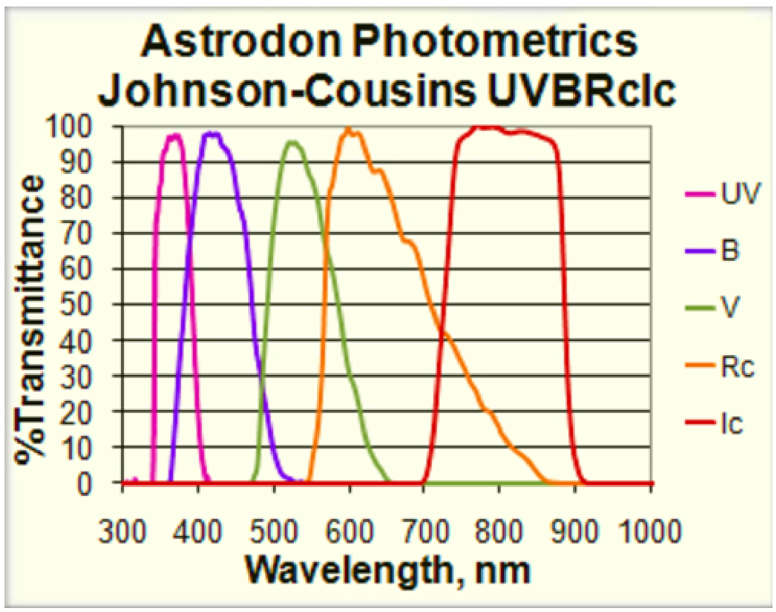

Figure 1.2 Various Johnson filters and corresponding wavelengths transmitted through them. Each filter allows wavelengths with varying transmittance as follows: UV, 340–410 nm; B, 375–525 nm; V, 475–650 nm; R, 550–860 nm; and I, 700–910 nm. Although five different filters are shown, we did not observe Mrk 501 in the ultraviolet (UV) range.This figure was taken from astrodon.com

high-energy wavelengths in 2012 and 2014. Even though flares appeared in both, the apparent correlations between high-energy and x-ray could have resulted from a time offset of ∼90 min between the VHE and x-ray telescopes. However, there is no correlation between the high-energy and the optical data (Cologna et al. 2016).

Aleksic et al. (2014) monitored Mrk 501 at a quiescent state, between March and May 2008, in wavelengths extending from radio to high-energy. During the campaign, all wavelength variations were stable—except x-ray. Even though x-ray varied, it was still below the average x-ray flux from December 2004–September 2012 ($\sim 2.0 \times 10^{-10}$ erg cm^{-2} s^{-1}). The x-ray and high-energy variations are correlated and comparable to a previous campaign in March 1996. They also found a trend showing that an increase in energy increases variability (Aleksić et al. 2015).

Kondo et al. (1981) conducted a project in which telescopes observing different wavelengths looked for variability in Mrk 501. They discovered that most of its energy emissions were in extreme UV (XUV). Although most emissions are found at XUV wavelengths, flares are found at other wavelengths as well. Since the flare in 1997, various flares in Mrk 501 have been observed: very high gamma, in 2009 (Neronov et al. 2012), 2012 (Cologna et al. 2016), and 2014 (Cologna et al. 2016) and (Chakraborty et al. 2016); and gamma and x-ray, in 2013 (Noda et al. 2015).

1.4 Work Done at BYU

Prior to my research at BYU, Mrk 501 had been observed in Johnson B, V, R, and I filters (Figure 1.2) since 2009 using Remote Observatory for Variable Object Research (ROVOR) (Moody et al. 2012) and West Mountain Observatory [(WMO) http://wmo.byu.edu/36inch/]. A previous undergraduate student, Marcus Holden, calibrated the data from ROVOR to put it on the same system as the WMO data (Holden Brigham Young University, Provo, U.T., 2016). This included applying flat, dark, and bias corrections so that frames were calibrated correctly for later photometry. When

I started research, optical (B, V, R, and I) wavelength data from calibrated frames were waiting to be extracted.

Chapter 2

Methods and Analysis

In this chapter, I describe how archived data can be compiled into a light curve and analyzed to find periodicity. I began working on the Mrk 501 project in January 2016. ROVOR data were scattered among many files throughout a computer called OLD YELLER. My first task was organizing frames of Mrk 501 according to day, month, and year. I found frames from April 2009 to April 2015 that I gathered and sorted according to the applied frame corrections: flat, bias, dark, light, etc. These corrections, referred to as calibrations, are used in photometry to get accurate measurements from observed objects. With the data gathered and sorted, I determined frames that were in need of calibrations to make necessary corrections. Once the data were calibrated, I could use them to create a light curve using *VPhot* and later *Mira*.

2.1 *VPhot*

Photometry is the act of extracting photon flux data from an object. *VPhot* (https://www.aavso.org/vphot), an excellent program for this task, is an online photometry program offered by American Association of Variable Star Observers (AAVSO). *VPhot* streamlines photometry by allowing the creation of telescope profiles containing specifications for each telescope: plate-scale, geographic coordinates, elevation, etc. After a telescope profile is created, frames can be uploaded to that profile subdirectory and grouped according to filter.

VPhot matches each frame to its World Coordinate System (WCS) coordinates. This allows *VPhot* to find the patch of sky corresponding to the uploaded frame. Once Mrk 501 is found from its RA and DEC (Section 1.1), the photon counts in a specified aperture are summed and compared against nearby catalogued stars on the frame. *VPhot* not only returns magnitudes, but also standard errors and signal to noise ratios (SNR) of each frame, which are helpful in determining uncertainty in measurements.

Our group decided to use *VPhot* because it is quicker than an individual analysis for each frame. A fast method of compiling a light curve was needed because some nights had hundreds of frames, requiring excessive amounts of time. I uploaded frames observed with ROVOR from 2009 to 2013, organized according to their filter type (B, V, R, and I). All uploaded frames appeared on the "images" page where a table is given showing useful information: telescope used, object observed, date and time taken, airmass, exposure time, and filter type. A few rows of this table are shown in Figure 2.1. Two important indicators, also shown, include whether or not all needed calibrations were applied and *VPhot*'s ability to plate-solve, i.e., whether *VPhot* could locate the frame on the WCS.

(a) Data uploaded from the WMO telescope. Mrk 501 was observed on June 13, 2015 for 120 s with a B filter. The indicators show that *VPhot* was able to plate-solve to WCS and were calibrated and used in a time series.

		Tele	Object	Date/Time	Airmass	Exposure	Filter	WCS	Cal	Rep
33		WMO	Mrk 501	2015-06-13 08:03:15	1.025	120 s	● B	■	■	■
32		WMO	Mrk 501	2015-06-13 07:44:13	1.013	120 s	● B	■	■	■

(b) Data uploaded from the ROVOR telescope. Mrk 501 was observed on July 7, 2009 for 90 s with an R filter. The indicators show that *VPhot* was able to plate-solve the first frames to WCS, but not the second. Both frames were calibrated, but only the top one was included in a time series. The bottom frame was unable to be included in a time series because it lacked WCS coordinates.

843		ROVOR RCO	MK501	2009-07-07 06:17:28	1.014	90 s	● R	■	■	■
842		ROVOR RCO	MK501	2009-07-07 06:11:34	1.011	90 s	● R	■	■	□

Figure 2.1 The above images are taken from *VPhot* showing organization of frames after being uploaded. Checkboxes in the left column are used for selecting frames to be included in a time series. A time series refers to a magnitude vs time graph, in which values are taken from a set of frames. The telescope, object observed, date and time of observation, airmass, exposure time of the telescope, and filter used are displayed in the table. The last three columns show green, red, yellow, and white indicators. A green indicator under "WCS" means that the WCS was able to plate-solve to the frame; red, unable. Yellow indicators under "Cal" means that the images were calibrated; white, not calibrated. Yellow under "Rep" affirms that data has been used in a time series; white, has not.

For frames in which *VPhot* was unable to plate-solve, I used *Astrometry.net* to locate and add the missing WCS information. After *Astrometry.net*'s addition of information to the file header, *VPhot* was able to find the WCS coordinates and analyze the frame. Only a few frames in 2013 data needed *Astrometry.net* to find WCS coordinates. With *VPhot*, only 2009-2013 data were uploaded because the 2014–2015 data were not calibrated. More thorough explanation of how *VPhot* and *Astrometry.net* were used in this project can be found in Rivest (2017, Brigham Young University).

2.2 *Mira*

In this section I explain the reason for using *Mira*, instead of *VPhot*. The photometry was done manually using predetermined, stable magnitudes of comparison stars to which I compared against Mrk 501. Some poor quality frames were captured, along with frames that were misoriented. Parameters for the aperture size were chosen and photometry was performed. I constructed a B, V, R, and I light curve with average nightly magnitudes of Mrk 501 from 2009–2013.

2.2.1 Setting Photometry Parameters

Using *VPhot* was convenient for the 2009–2011 frames, however the 2013 data had too many plate-solving errors. In addition to the plate-solving problem, some frames were unsolvable even after putting them through Astronometry.net. Because of the problems from the 2013 data and not understanding how *VPhot* determines its light curves, I decided to individually phot (perform photometry) the ROVOR data using *Mira*. This method took longer, but allowed me to learn the skills of manual data reduction. *Mira* includes a photometry package that was utilized in determining magnitudes of different objects.

For the *Mira* data, I decided which frames were included in the photometry and which were removed due to poor image quality (Section 2.2.2). After the desired frames were chosen, *Mira* used an aperture and annulus, shown in Figure 2.2, to gather data from the frames. Object counts were summed in the inner aperture (the red circle surround by the dashed teal circle), and background counts were calculated from the annulus (the blue region between the outside red circles) and subtracted from object counts.

The photometric parameters, depicted in Figure 2.3, being aperture radius, annulus inner and outer radius, and eccentricity, were adjusted to fit around the target's image. I used a circular aperture (eccentricity of 1). After setting the parameters, standard objects, i.e., objects stable in magnitude, were chosen. If more than one frame was photed, a tracking function was implemented effecting the aperture centroids to follow their targets from frame to frame. If an object's coordinates moved drastically far between frames, then the tracking function missed its target and I would manually drag the parameters onto desired targets.

Mira used these parameters to determine the targets' relative brightness. Each of these three parameters summed the number of photon flux counts corresponding to a given area. The smallest circle (aperture) encompassed the target and summed counts within its area. The annulus summed the counts for the background in the area between the two outer circles. These magnitudes were used in finding the target's apparent magnitude.

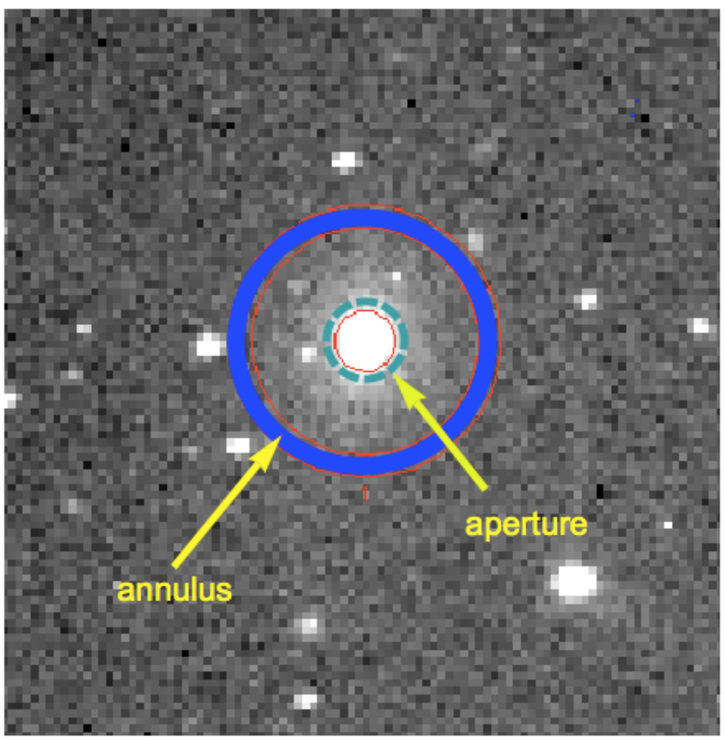

Figure 2.2 Image from *Mira* showing the aperture and annulus. The aperture, at the center, is the middle red circle surrounded by a dashed, teal circle. The aperture encircles Mrk 501 to obtain its magnitude. The annulus is marked with a thick, blue ring between the two outer, red circles. The annulus is used to obtain the average background magnitude to determine relative brightness of Mrk 501.

2.2.2 Differential Photometry

Using the aperture function, shown in Figure 2.3, I found parameters that encircled Mrk 501 on the frame of 4 (aperture radius), 15 (inner ring radius), and 18 (outer ring radius) pixels. This good fit can be seen where the aperture (center red circle) fits well around the bright Mrk 501 image. An ensemble of two nearby stars was used for comparison stars, which I refer to as Star 1 and Star 4 throughout this thesis. These two stars are depicted in Figure 2.4 as "1" and "4" with a table, in Figure 2.5, showing their average magnitudes in B, V, R, and I filters. These values of magnitude for observations were entered into *Mira*. In Figure 2.6, the average magnitude of Star 1 observed in the R filter was entered into *Mira*. These comparison stars were chosen for their stability to a few hundredths of a magnitude. Their stability makes them the best ensemble for differential photometry of Mrk 501 (Pace et al. 2013).

After photing the frames with the parameters and comparison star magnitudes above, *Mira* returned apparent magnitudes for Mrk 501—for each frame. I copied all the values into Microsoft *Excel*, and I found three differential magnitudes (for a given frame) by differencing the magnitudes between Mrk 501 with Star 1 (δ_{M1}), Mrk 501 with Star 4 (δ_{M4}), and Star 1 with Star 4 (δ_{14}) as shown in Eqs. (2.1), (2.2), and (2.3) below:

$$\delta_{\mathrm{M1}} = \mu_{\mathrm{M}} - \mu_1 \tag{2.1}$$

$$\delta_{\mathrm{M4}} = \mu_{\mathrm{M}} - \mu_4 \tag{2.2}$$

$$\delta_{14} = \mu_1 - \mu_4 \tag{2.3}$$

The variable μ has been chosen to represent magnitude, therefore μ_a would be short for magnitude of a. The δ_{ab}, likewise represents a shift between two things (magnitude of objects, filters,

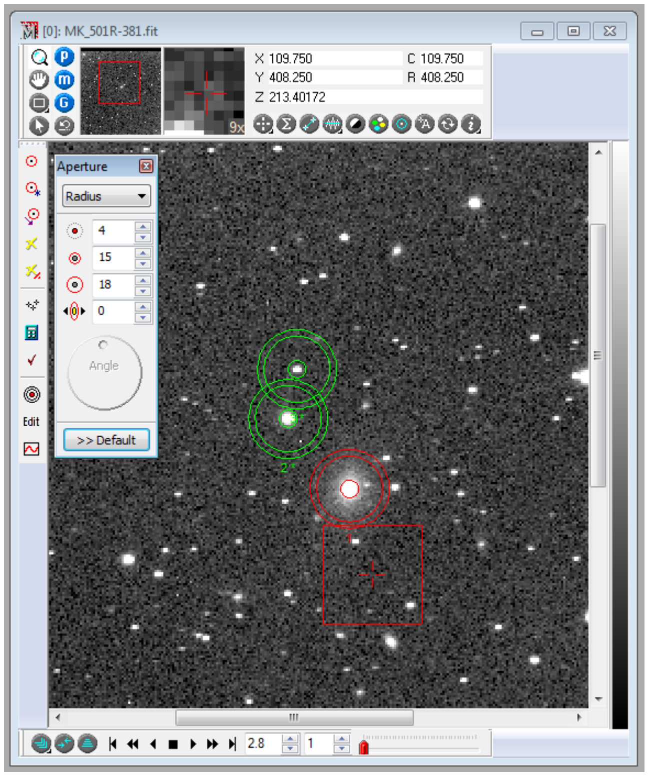

Figure 2.3 The parameter pixel radii can be changed on *Mira*. The first input (4 pixels) is for the aperture, the second and third inputs (15 and 18 pixels) change the size of the annulus. The last input box is for choosing eccentricity of the aperture and annulus and remained at 0 (eccentricity = 1) throughout this project. The ">> Default" button is used to save the above apertures as a default values that can be used later. The aperture is used to sum the number of counts enclosed in the smallest red or green circle. The annulus sums the number of counts between the two outer circles for a background reading to be compared against the aperture counts and determine and apparent magnitude of the object in the aperture.

telescopes, etc.), a and b. The "M" is shorthand for Mrk 501. Averaged values have a bar over them, e.g. the average magnitude of Mrk 501 is $\overline{\mu_M}$, and are equivalent to using *Excel*'s AVG on all apparent magnitudes of Mrk 501 for a given night. If the equation was $\overline{a \cup b \cup c}$ that would be equivalent to using AVG(A1:A10 [a's] , B1:B10 [b's], C1:C10 [c's]) in *Excel*, which gives the average of all a's, b's and c's together. These and other notations can be found in Appendix A.

I used *Excel*'s AVG and STDEV functions to determine nightly averages of δ_{M1} ($\overline{\delta_{M1}}$), δ_{M4}

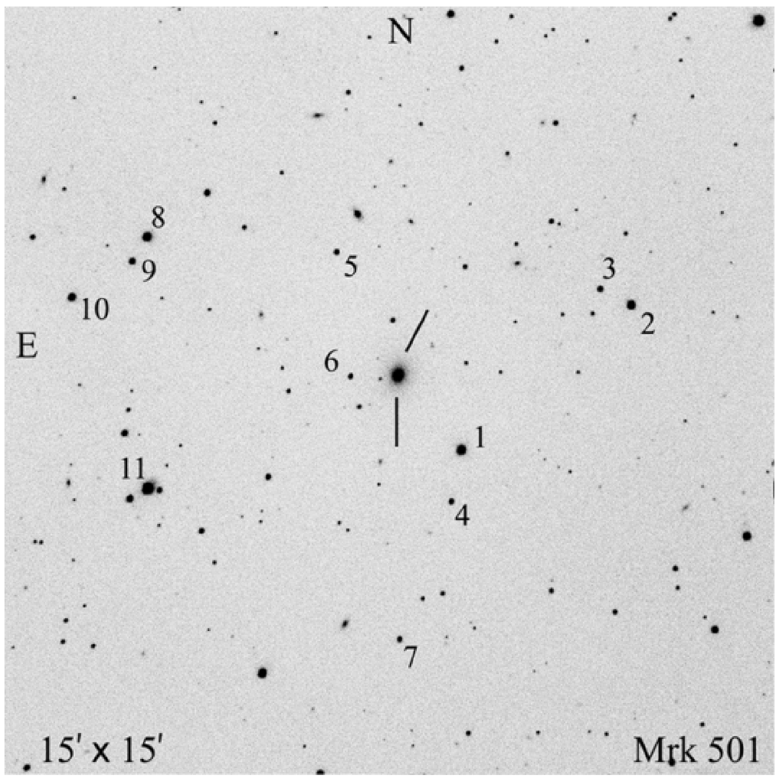

Figure 2.4 Frame taken of the sky surrounding Mrk 501, with Mrk 501 at the center. The frame size is 15′ (arc min) by 15′. Each comparison star is marked with number. We only used comparison stars "1" and "4" (found southwest from Mrk 501). Figure taken from Pace et al. (2013)

.

Figure 2.5 Various host galaxies and their most stable comparison stars found in the nearby sky. Average magnitude values for comparison stars are shown for B, V, R, and I filters. When photing, I used the values for Star 1 with magnitudes: B = 13.540, V = 12.598, R = 12.083, and I = 11.613 and for Star 4: B = 15.961, V = 15.309, R = 14.931, and I = 14.572. Table from Pace et al. (2013).

Table 2.
ESTIMATION OF PHOTOMETRIC VALUES FOR DEMONSTRABLY STABLE STARS

Field	Star	$B(\sigma)$	$V(\sigma)$	$R(\sigma)$	$I(\sigma)$	Other designations
MRK 421	1	14.982 (0.009)	14.384 (0.006)	14.022 (0.004)	13.692 (0.003)	
	2	16.173 (0.010)	15.571 (0.007)	15.200 (0.004)	14.866 (0.005)	3[5]
	4	15.135 (0.010)	14.124 (0.006)	13.534 (0.004)	13.018 (0.004)	8[5]
	5	14.390 (0.012)	13.571 (0.006)	13.062 (0.004)	12.628 (0.004)	2[5]
H 1426+428	1	15.61 (0.02)	14.16 (0.01)	13.25 (0.01)	12.46 (0.01)	A[2]
	2	15.45 (0.02)	14.60 (0.01)	14.15 (0.01)	13.76 (0.01)	B[2]
	3	14.20 (0.01)	13.40 (0.01)	12.99 (0.01)	12.61 (0.02)	C[2]
MRK 501	1	13.540 (0.003)	12.598 (0.003)	12.083 (0.003)	11.613 (0.001)	5[1]
	4	15.961 (0.018)	15.309 (0.010)	14.931 (0.009)	14.572 (0.010)	3[1]
1ES1959+650	1	13.359 (0.012)	12.686 (0.012)	12.280 (0.004)	11.916 (0.004)	
	2	13.446 (0.014)	12.888 (0.008)	12.534 (0.004)	12.217 (0.004)	
	4	15.277 (0.014)	14.501 (0.008)	14.038 (0.004)	13.619 (0.004)	
	6	15.968 (0.015)	15.204 (0.012)	14.758 (0.004)	14.365 (0.004)	
	7	16.001 (0.015)	15.225 (0.012)	14.738 (0.004)	14.315 (0.004)	
BL Lac	1	14.643 (0.020)	12.936 (0.011)	11.966 (0.014)	11.105 (0.016)	B[3,4], 12[1,6]
	2	15.178 (0.012)	14.278 (0.008)	13.760 (0.011)	13.313 (0.013)	C[3,4], 21[1,6]
	3	15.723 (0.017)	14.452 (0.004)	13.695 (0.013)	13.024 (0.009)	H[3,4], 16[1,6]
	4	16.380 (0.021)	15.549 (0.009)	15.051 (0.009)	14.561 (0.010)	K[3,4], 17[1,6]
	5	15.484 (0.026)	14.439 (0.007)	13.797 (0.010)	13.237 (0.013)	3[1,6]
	6	14.327 (0.023)	13.298 (0.004)	12.689 (0.006)	12.161 (0.015)	25[1,6]
	8	15.097 (0.008)	14.254 (0.016)	13.755 (0.017)	13.262 (0.020)	28[6]
	9	15.144 (0.013)	14.191 (0.020)	13.590 (0.017)	13.070 (0.023)	29[6]

[1] Doroshenko et al. (2005)
[2] Smith et al. (1991)
[3] Villata et al. (1998)
[4] Smith et al. (1985)
[5] Bertaud et al. (1969)
[6] González-Pérez et al. (2001)

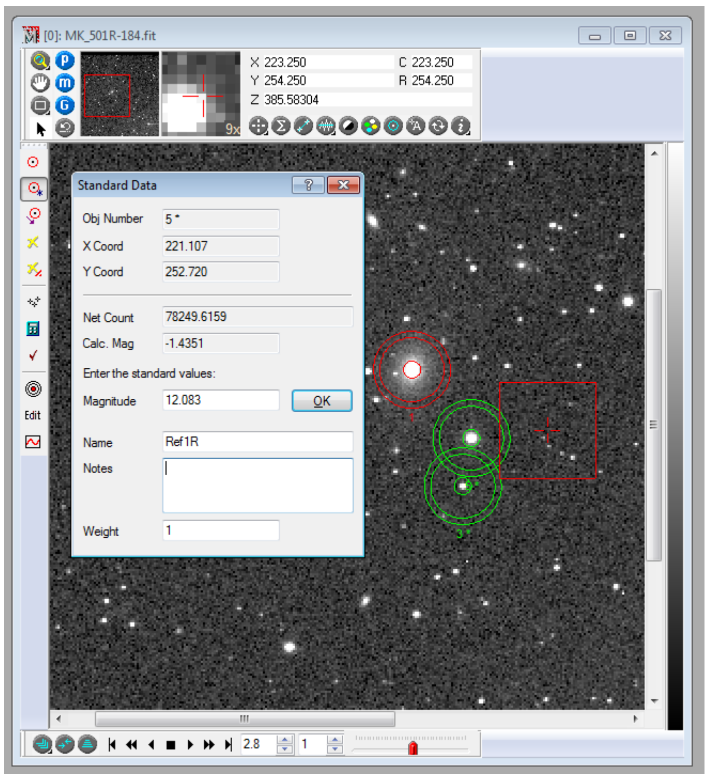

Figure 2.6 Stable values of Star 1 from Figure 2.5 were entered in *Mira*. Known values for the comparison stars were used to find the apparent magnitude of Mrk 501. The value of Star 1 for the R filter was 12.083 mag.

($\overline{\delta_{M4}}$), and δ_{14} ($\overline{\delta_{14}}$) and corresponding standard deviations. I added Star 1's magnitude with the nightly average value to find the average magnitude of Mrk 501 each night as shown in Eq. (2.4):

$$\overline{\mu_M} = \mu_1 + \overline{\delta_{M1}} \tag{2.4}$$

The standard deviations were used to determine the intra-night variability (Section 1.3) of Mrk 501's magnitude. I used Eq. (1.1) to find the average magnitude of Mrk 501 each night in a given filter (with few exceptions that are described later).

The aperture parameters of 4, 15, and 18 pixels were only used for the 2013 data because of the difference in binning of pixels from year to year, as shown in Figure 2.7. The left figure shows the aperture size from 2013 to be 4, 15, 18 pixels and a frame size of 512 $\times$ 512 pixels, while the right figure (from 2010) had 1024 $\times$ 1024 pixels. Because of the difference in frame size, I doubled the parameters, ensuring the same enclosed area on the frame as the 2013 data. The parameters used from May 2009 through 2011 were 8, 30, 36 pixels.

Frames Withdrawn from Data Set

For many reasons, there were nights that had frames containing abnormalities that could not be used in photometry. Some frames were saturated from the sunset, as in Figure 2.8, resulting in white images. Occasionally cloud cover blocked the night sky, shown in Figure 2.9, causing poor object visibility. When cosmic rays from the jet contacted the charged-coupled device (CCD) as depicted in Figure 2.10, the value of a pixel drastically increased/decreased effecting misreadings on pixels. Sometimes Mrk 501 was not visible on the frame as in Figure 2.11, but showed Mrk 421 (another galaxy) instead. In rare instances, images were missing the flat correction like that shown in Figure 2.12, which were removed because of the values returned. These corrupted frames effected the presence of huge outliers or yielded no extractable data, therefore I removed them before photing. Examples of such frames are shown in Figs. 2.8–2.12.

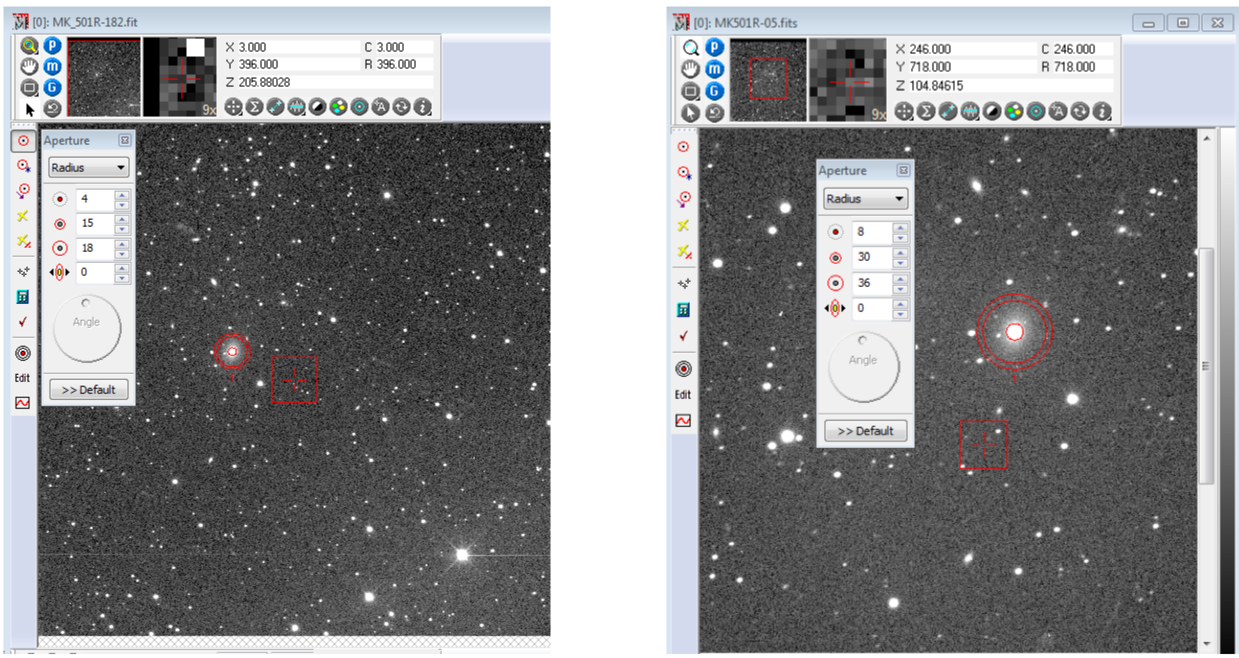

Figure 2.7 Different years required a different aperture size. The left figure was from 2013 with aperture parameters of 4, 15, and 18 pixels. The right figure was from 2010 with parameters of 8, 30, 36 pixels. A difference in object size between the two frames can be seen.

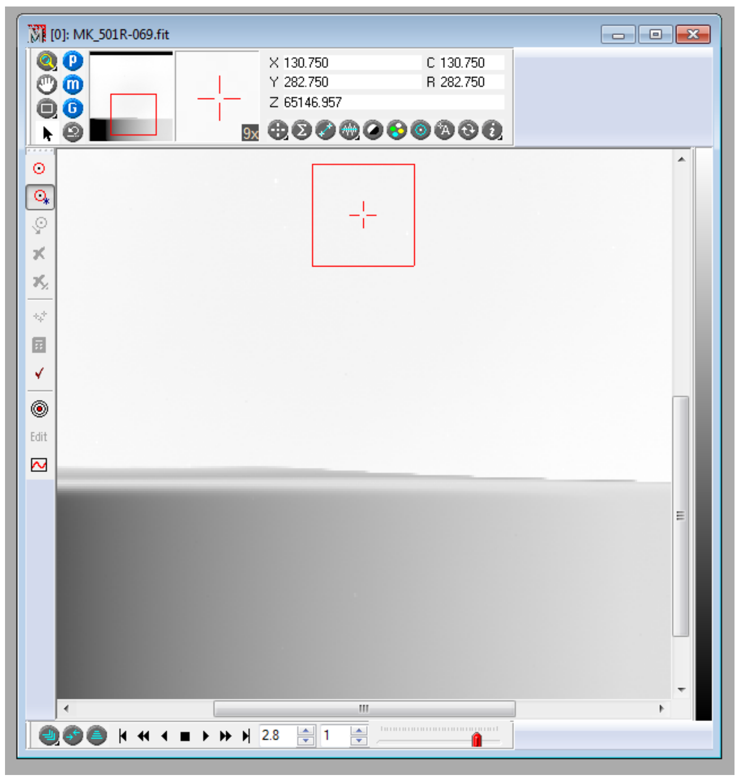

Figure 2.8 Saturated frame (probably taken in the morning). Some frames gradually brightened until the frame would appear white. This saturation was caused from the brightness of a sunrise. No data could be retrieved using *Mira* for these frames so they were not included in the analysis.

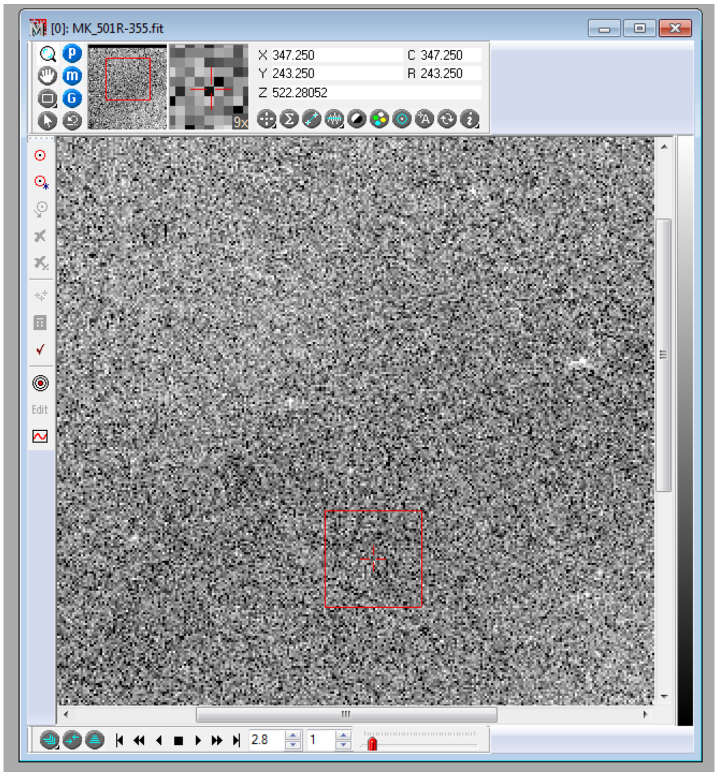

Figure 2.9 Cloudy night with very few visible stars. When cloud cover was on a frame, *Mira* was unable to accurately measure magnitudes. Only cloud-free nights were used.

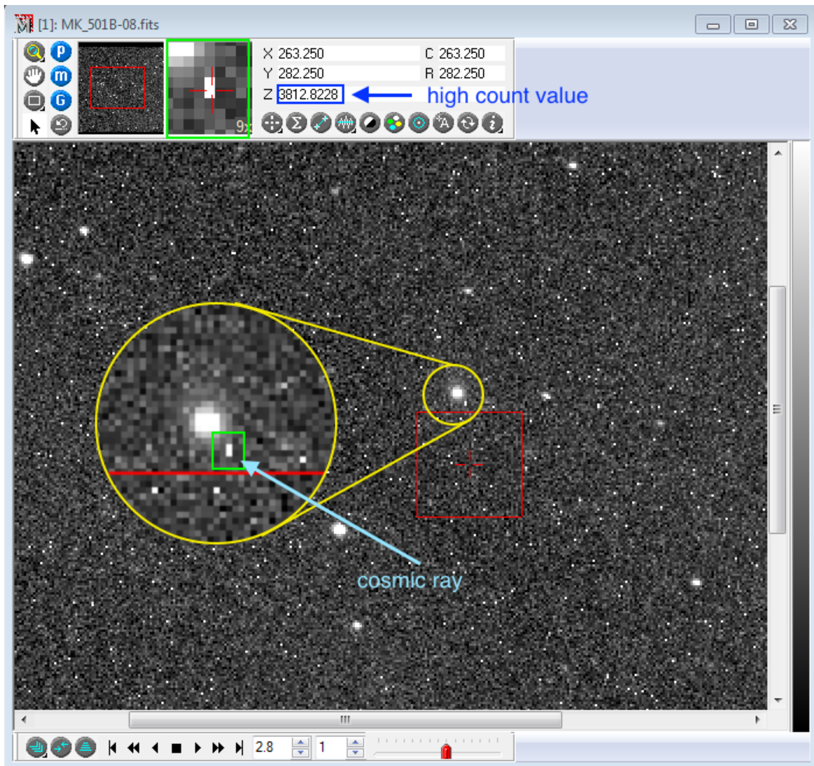

Figure 2.10 Frame containing cosmic rays. The area containing the cosmic rays has been enlarged for clarity. These pixels (pointed out with a light blue arrow) were effected by cosmic rays contacting the charge-coupled device (CCD). Because of the extreme energy flux from these particles, affected pixel counts (in the blue box) were off by orders of magnitude. The cursor (in the green box) was placed over the affected pixel to show their flux count values. The aperture and annulus' measurements were inaccurate, affecting readings for background and Mrk 501's apparent magnitude. These frames were also removed because of their enormous outliers.

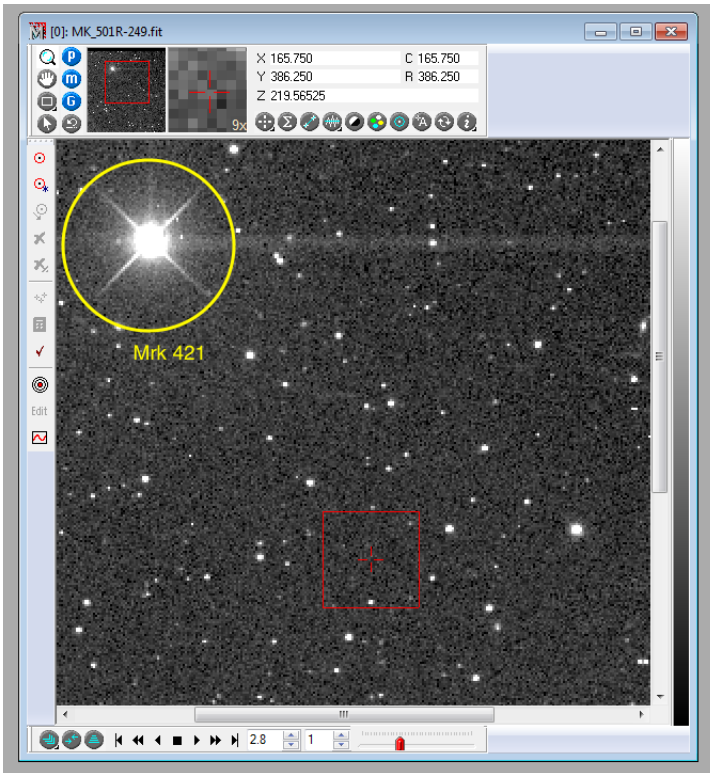

Figure 2.11 Frame showing Mrk 421, instead of Mrk 501. A few times Mrk 421 (circled in yellow) was shown in the frame and lacked the presence of Mrk 501. This temporary switch of targets is believed to have taken place when students were learning how to use ROVOR. No data were retrieved and these frames were not used.

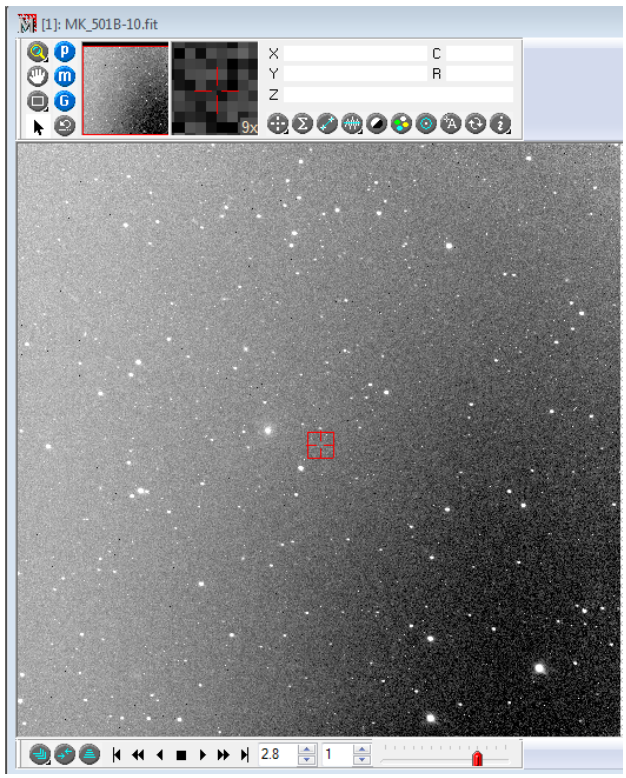

Figure 2.12 Frame bereft of its flat correction. Frames without an applied flat field also cause outliers and were removed. The image does not look smooth and there are dark and light patches of sky. Unflattened frames were also left out from analysis.

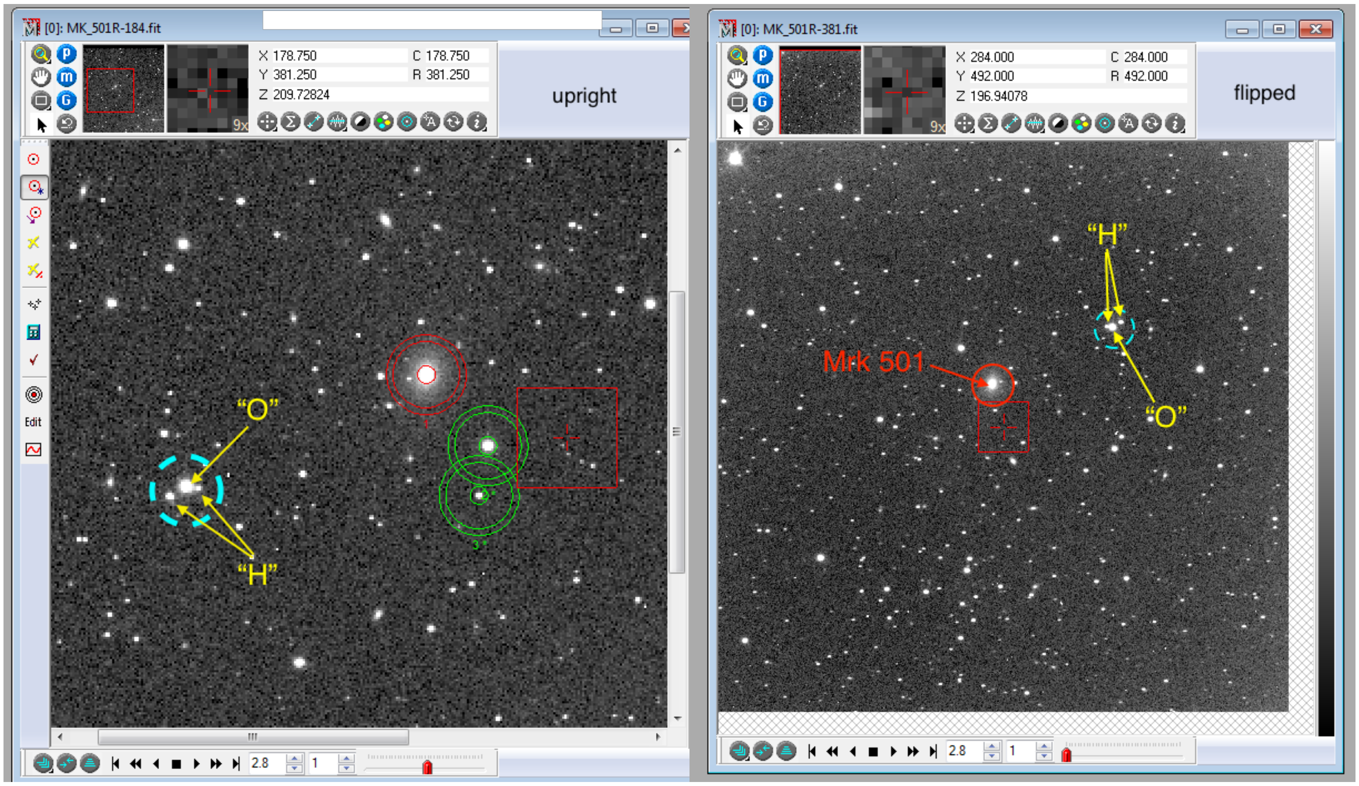

Figure 2.13 The orientations of both flipped and upright frames. The upright image is on the left with the "molecule," (surrounded by the dashed, light blue circle), on the bottom left side with "oxygen" above the "hydrogens." The flipped image is on the right with the "molecule" on the top right corner where "oxygen" is below the "hydrogens."

Flipped Frames

The telescope flipped over the pier a few times showing different orientations of inverted frames. Many frames were flipped vertically requiring me to apply a correction to the observed magnitudes of Mrk 501, so that the flipped magnitudes matched the upright ones. To specify what vertically flipped means, on a frame there is a cluster of stars resembling a water molecule (circled in a dashed, light blue circle), as seen in Figure 2.13. If the two smaller stars (hydrogen on the water molecule) were below the bigger one (oxygen) and the cluster was in the bottom left portion of the frame, as in the left figure, the frame was upright. If the molecule was in the top right corner with the "hydrogens" above the "oxygen," as in the right figure, the frame was considered flipped.

Whenever a night had two orientations (upright and flipped), photometry was done on each separately as described in Section 2.2.2. To correct the flipped frame the following calculation was performed in Eq. (2.5):

$$C = |\overline{\delta_{M4_{(f)}}}| + (\overline{\delta_{14_{(u)}}} - \overline{\delta_{14_{(f)}}}) \tag{2.5}$$

The correction to the flipped frame C is used to correct the slight offset in magnitude that arises when upright and flipped frames are photed and compared. The added subscripts *(u)* and *(f)* refer to the orientation of the frames, where *(u)* is measured in the upright frame and *(f)* in the flipped frame.

To match the flipped data with the upright I added C to the to the average value of δ_{M1} in the flipped frame. After getting the shifted value for the flipped data, I averaged the flipped and upright data and then added the magnitude of Star 1 to get the average magnitude of Mrk 501 [Eq. (2.6) below]:

$$\overline{\mu_M} = \overline{\delta_{M1_{(u)}} \cup (\delta_{M1_{(f)}} + C)} + \mu_1 \tag{2.6}$$

Mrk 501's average magnitude over a night is $\overline{\mu_M}$ (a detailed explanation of notation is given in Appendix A). For data between May 2009–July 2009, I defined another orientation for the mirrored frames (rotated 180° out of the page) shown in Figure 2.14. The left figure shows the upright orientation, defined as having the "molecule" on the right side with the "hydrogens" above "oxygen." The right figure shows the flipped frame, having the "molecule" on the left with "oxygen" above the "hydrogens." After deciding the new orientations, Eq. (2.5) was implemented to shift the flipped data to match the upright.

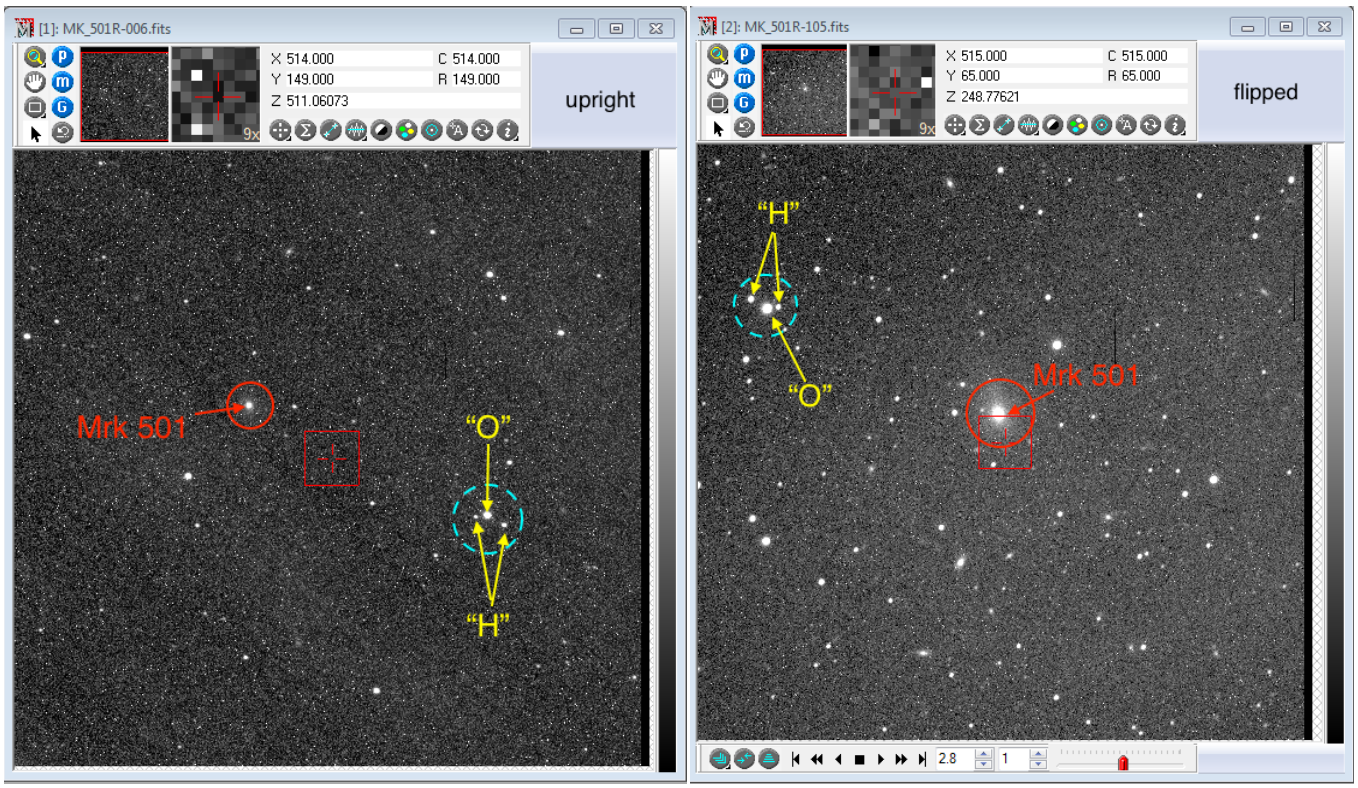

Figure 2.14 Orientations of both flipped and upright frame for the mirrored-flip. The upright frame is the left figure with the "molecule" (surrounded by the dashed, light blue circle) on the bottom right side of the frame with "oxygen" above the "hydrogens." The flipped image is on the right with the "molecule" on the top right corner and "oxygen" below "hydrogens."

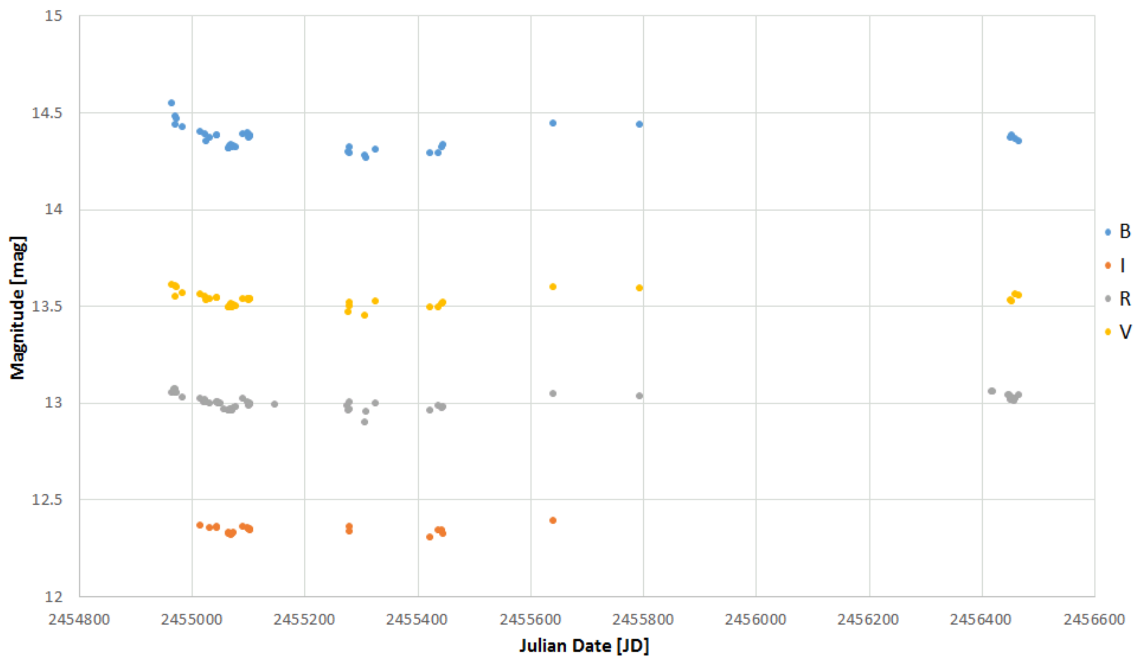

Figure 2.15 Light curves of each filter (B, V, R, and I) from 2009–2013. Because of the reverse log-scale, smaller magnitudes represent brighter data points. Each of the filters and their respective magnitudes were plotted. A trend is apparent as data form similar maxima and minima for each filter, despite variation in spread. Offsets among filters are later removed to show a more apparent pattern. (cf. Figure 2.16).

2.2.3 Light Curve for 2009–2013 ROVOR Data

Assembling the Photometry and Color Differentials

Next, I gathered the data to compile light curves for B, V, R, and I filters, individually. A light curve is a graph showing how magnitude of an object changes over time. Having photed all of ROVOR's frames, I plotted each $\overline{\mu_M}$ (y-axis) versus average Julian Date (AJD) from 2009–2013 shown in Figure 2.15. In each of the filters, similar maxima and minima were shared. These patterns that appeared in each filter were later analyzed after removing the offset by shifting the data to a common filter. This enabled me to verify the oscillations among filters.

Shift to V Filter

I removed offsets from V to each filter to more clearly see how individual light curves overlapped by: first, determining the average magnitudes of B, R, and I filters; then subtracting V from those magnitudes, to find the average offset; and finally, adding that offset to each nightly magnitude of B, R, and I filters. This process is demonstrated by Eqs. (2.7)–(2.12):

$$\overline{\delta_{BV}} = \overline{B} - \overline{V} \tag{2.7}$$

$$\overline{\delta_{VR}} = \overline{V} - \overline{R} \tag{2.8}$$

$$\overline{\delta_{VI}} = \overline{V} - \overline{I} \tag{2.9}$$

$$B_{(V)} = B - \overline{\delta_{BV}} \tag{2.10}$$

$$R_{(V)} = R - \overline{\delta_{VR}} \tag{2.11}$$

$$I_{(V)} = I - \overline{\delta_{RI}} \tag{2.12}$$

The average offsets between the different filters and V is shown by $\overline{\delta_{filter1filter2}}$. The average values of all the data in a given filter is shown by $\overline{B}$, $\overline{V}$, $\overline{R}$, and $\overline{I}$. The B, R, and I represent applying a specific shift to all the data in its filter. The subscript *(V)* means that the B, R, and I have an offset applied to the B, R, and I filter magnitudes so that they line up with V. With B, R, and I filters at the same average magnitude of V, I plotted the new light curve with $B_{(V)}$, $R_{(V)}$, $I_{(V)}$, and V together in Figure 2.16, and verified the apparent trend in Figure 2.15.

A Common Trend

After all the data were plotted, a pattern could be seen in Figure 2.16. In the beginning of this light curve, the average magnitude of Mrk 501 was at a minimum among the four filters. As time

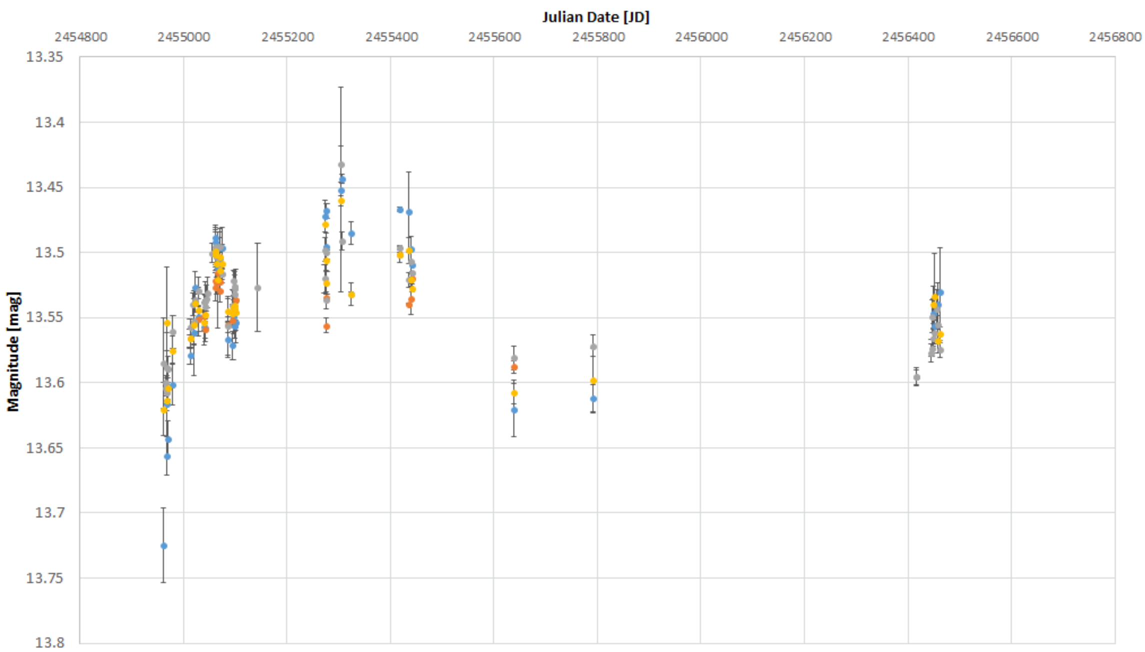

Figure 2.16 Modified light curve from 2009–2013 with the offsets from V removed (cf. Figure 2.15). Years have been added showing when Mrk 501 was observed. Magnitudes (y-axis) are now shown in reverse order with top values being brightest. Each of the filters have the same periodicity in magnitude variations. In 2009, the magnitudes are at a minimum, that is clearest to see in the B filter. Around 2010, the light curve reaches its maximum. In 2011, although there were few points, the data appears at a minimum comparable to the 2009 data. From 2011 to 2013 the magnitudes increase. The overall trend appears to be sinusoidal in nature.

progressed to 2010, Mrk 501 brightened with a maximum around April 2010. After this peak, the magnitude decreased with another minimum brightness in 2011, slightly higher than the 2009 values. No data were taken in 2012. However, in order to increase from 2011 to 2013, 2012 magnitudes must have been higher than 2011 to reach the values in 2013. This pattern is possibly sinusoidal, but I had questions concerning the low magnitude values in 2009 and larger outliers. I took a few more steps to make sure the data were correct.

2.2.4 Verifying Light Curve Data

A New Aperture for the Earlier CCD

Because of the drop in the magnitudes for all filters in 2009, to guarantee that the data were accurate with the other years, I photed the 2009 data again using parameters of 8, 30, and 36 pixels obtaining the same results. I noticed that frames from May 2009 had different pixels dimensions than the later 2009 data. This was because in June 2009, the CCD was changed in ROVOR, requiring me to use different photing parameters. The old CCD frames were binned differently and had a frame size of 512 $\times$ 528 pixels (as opposed to 528 $\times$ 528 pixels). These photometric parameters were slightly different from the 8, 30, 36 pixels, and could not be scaled as I did for the difference in the 2013 and 2011–June 2009 aperture. I found that using 7.385, 27.692, and 33.321 pixels for parameters took up, relatively, the same amount of area. I used this more accurate aperture to phot the May 2009 data again.

Reference Star Stability

As important as it was to make sure the parameters were correct, it was also important to verify the magnitude stability of the comparison stars (Star 1 and Star 4) throughout the observations. Figure 2.17 illustrates the stability between Star 1 and Star 4. I plotted the standard deviation of δ_{14} for each night vs average JD. The graph showed that during 2009–2013 (excepting one R data

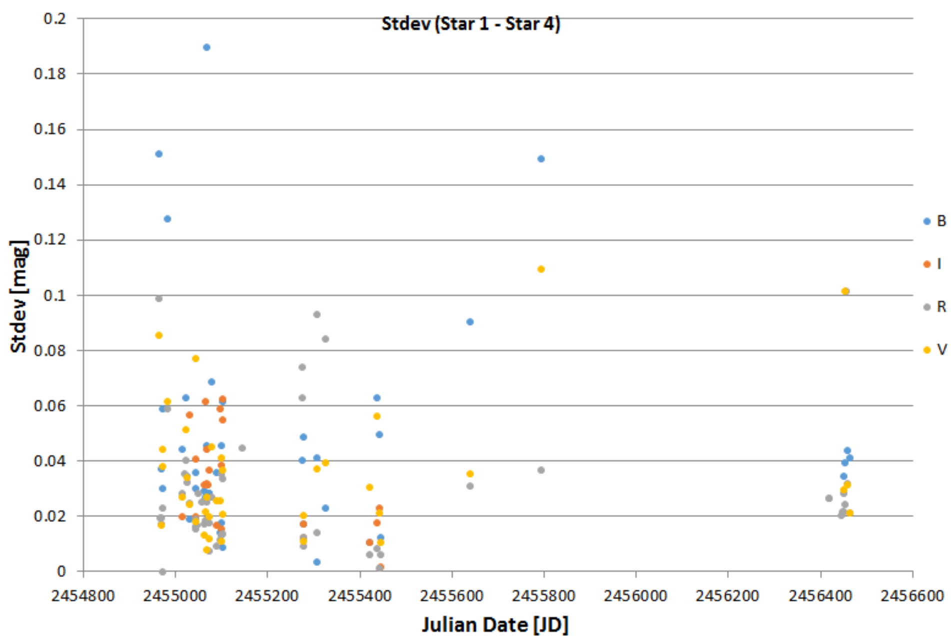

Figure 2.17 Variability in the two comparison stars (Star 1 and Star 4) during 2009. The y-axis shows the values of the nightly standard deviations between Star 1 and Star 4 with the x-axis as average JD. Although the data spreads with the outliers present the average magnitudes are quite small: B, 0.049; V, 0.036; R, 0.029; and I, 0.033 mag. I concluded that the comparison stars are stable to few hundredths of a magnitude, similar to the variability found by Pace et al. (2012).

point that had a value of 0.47 mag) the nightly standard deviations ranged from 0.001–0.189 mag. Although there a few outliers, the standard deviations average is low with: B, 0.049; V, 0.036; R, 0.029; and I, 0.033 mag (data in Appendix B). With these results, I concluded that the comparison stars were stable and were not misrepresented in the light curve.

A New Method of Correcting Flipped Frames

I implemented a more accurate way to find magnitudes of flipped images. Instead of using the nightly average for flipped frames (as in Section 2.2.2), I used the photon flux counts of Mrk 501 for one flipped and upright frame. I found where in the sequence the frames transitioned from upright to flipped or vice versa. I extracted the number of counts for both upright and flipped and took the absolute difference between counts. I used Eq. (1.1) to convert counts to a magnitude. Then I added this magnitude to $\overline{\mu_{(f)}}$ to get the correction in the flip. These steps are shown below.

$$\delta_N = |N_{(u)} - N_{(f)}| \tag{2.13}$$

$$C = 2.5 \times \log_{10} |\delta_N| \tag{2.14}$$

The number of counts of Mrk 501 is N and the difference in counts is notated by δ_N. Once again, C is the correction to the flipped frames. After applying Eqs. (2.13) and (2.14), Eq. (2.6) can be implemented to find the average magnitude of Mrk 501 as described in Section 2.2.2. These equations allowed for a more consistent and accurate shift in magnitudes from flipped frames to upright.

2.2.5 *Peranso* Analysis

After extracting ROVOR data from 2009–2013, I met with Joe (who was also working on the Mrk 501 project) to perform frequency analysis. While I was photing the ROVOR data using *Mira*, Joe was photing WMO data using *VPhot* (Rivest Brigham Young University, Provo, U.T., 2017). We plotted ROVOR and WMO together in B, V, and R filters, respectively, and using the frequency analysis program, *Peranso* (www.peranso.com), found a long-term period of 113 days in optical wavelengths. No I filter observations were taken by WMO, so we left the I filter data out of the project. When we put the data together, there was an apparent offset between magnitudes of WMO and ROVOR. We were surprised to see that between similar filters, the apparent magnitudes of the two telescopes differed by 0.2–0.5 mag. There should not be a difference between telescopes with the same filters observing the same object, unless it is instrumental. To make sure that the photometry was correct more work needed to be done.

2.3 ROVOR/WMO Offset

2.3.1 Five Arcsec Aperture

To ensure the similar photometry was performed on telescopic data sets, the same aperture and annulus size were used for both *VPhot*'s photing of WMO and *Mira*'s photing of ROVOR. We decided to use an aperture size of 5” (arcsec) because 5” is the most common aperture used on Mrk 501. This yielded new parameters for *Mira* of 1.85, 15, and 18 pixels. When comparing the size of the 1.85 pixels (5”) aperture, shown in Figure 2.18, with the 4 pixels aperture (Figure 2.7), it is apparent that the 5” aperture more accurately encircles Mrk 501's core. It was not only requisite for aperture sizes to be identical, but we also needed the same ensemble of comparison stars.

2.3.2 New Ensemble of Five Stars

Instead of using two stars again for the ensemble, we used five. These five stars were used when photing in *VPhot* and *Mira*. The new five star ensemble is shown in Figure 2.19 for *Mira* and Figure 2.20 for *VPhot*. One of the stars in this new ensemble was in the original ensemble (cf. Figure 2.3). In Figure 2.19, the ensemble consists of stars that are labeled 2–6. The star labeled "2", at the center of the frame, is the same star as Star 1 from the first ensemble in Figure 2.3.

In *VPhot*, we used this ensemble (as shown in Figure 2.20) that is identical to Figure 2.19. The five comparison stars are given the labels "Star 1", "126", "132", "144", and "148." This Star 1 (on *VPhot*) is not the same as the star that I have been calling Star 1 from Pace et al. (2012). The original Star 1 (in the first ensemble) is given the label "126" in this image. The parameters to obtain a 5” aperture are different in *VPhot*, having values of 8.2, 14, and 66 pixels. The 14 pixels does not refer to the radius of the inner circle of the annulus, it refers to the width of the annulus, so 14 would mean an inner radius of the annulus of 52 pixels.

Along with the five comparison stars, *VPhot* also created a chart, depicted in Figure 2.21,

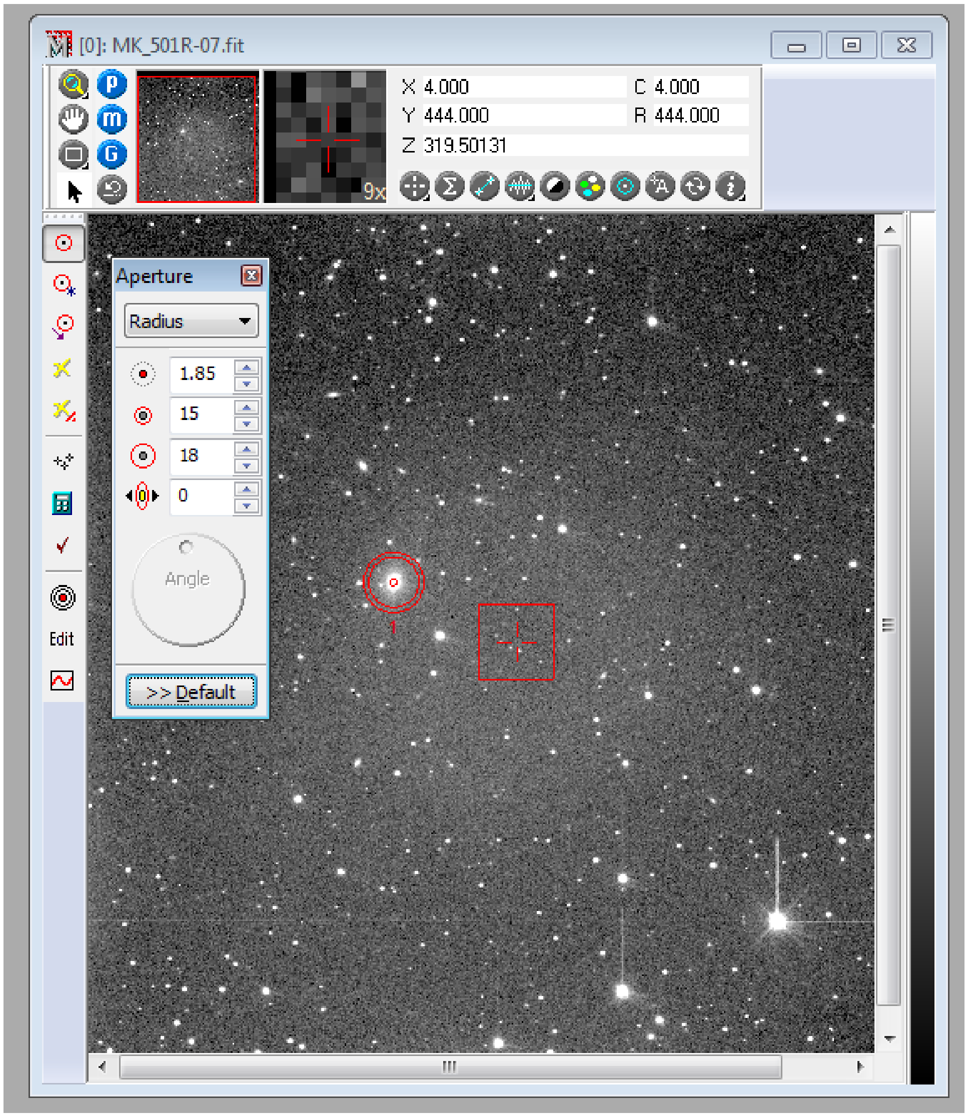

Figure 2.18 Frame from ROVOR with the 5” aperture around Mrk 501. The 5” aperture focuses on the core of Mrk 501, while the previous 4, 15, 18 pixels aperture choice focused on the galaxy as a whole (cf. Figure 2.7). In literature, Mrk 501 is usually monitored with a 5” aperture.

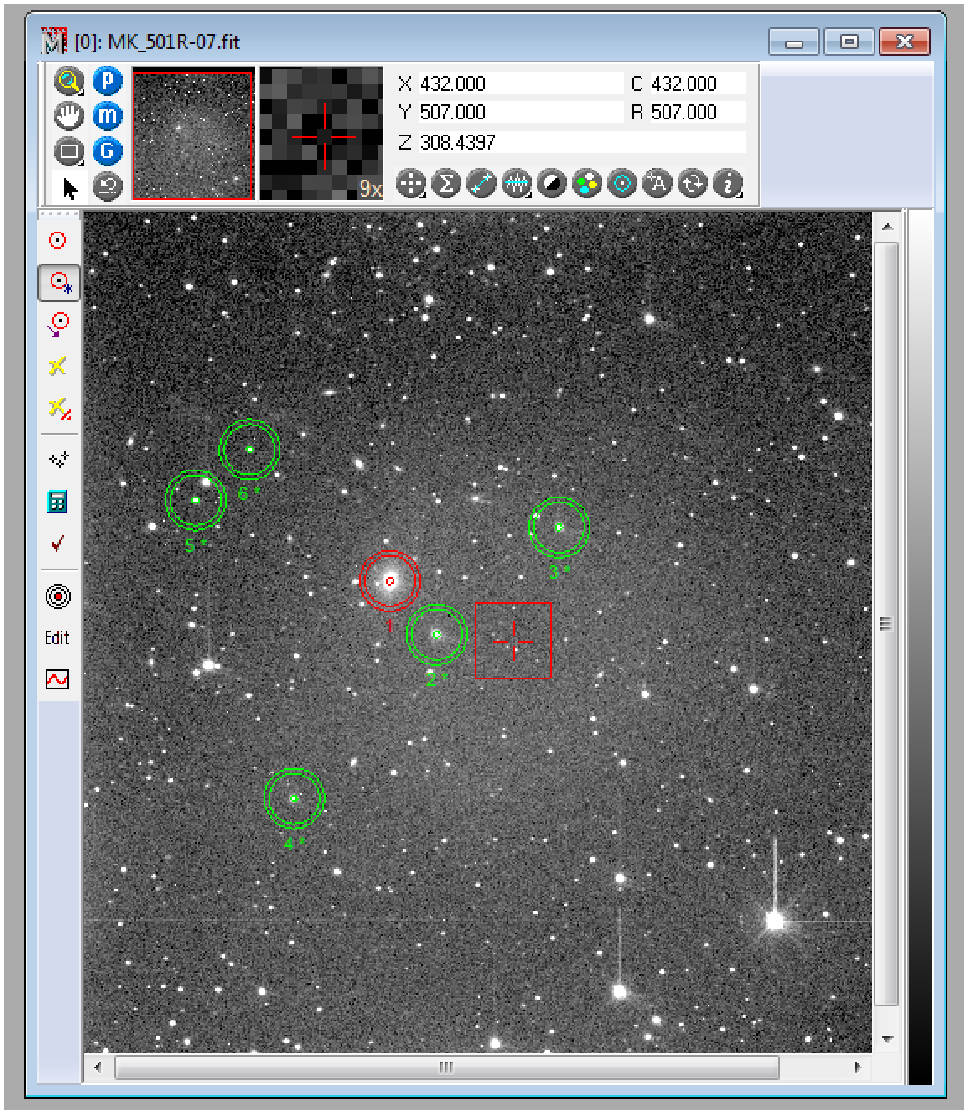

Figure 2.19 The new five star ensemble with stars encircled in *Mira*. The comparison stars are numbered from 2–6, encircled in green with Mrk 501 in red. The star, "2," is the same as Star 1 from the two star ensemble (cf. Figure 2.3).

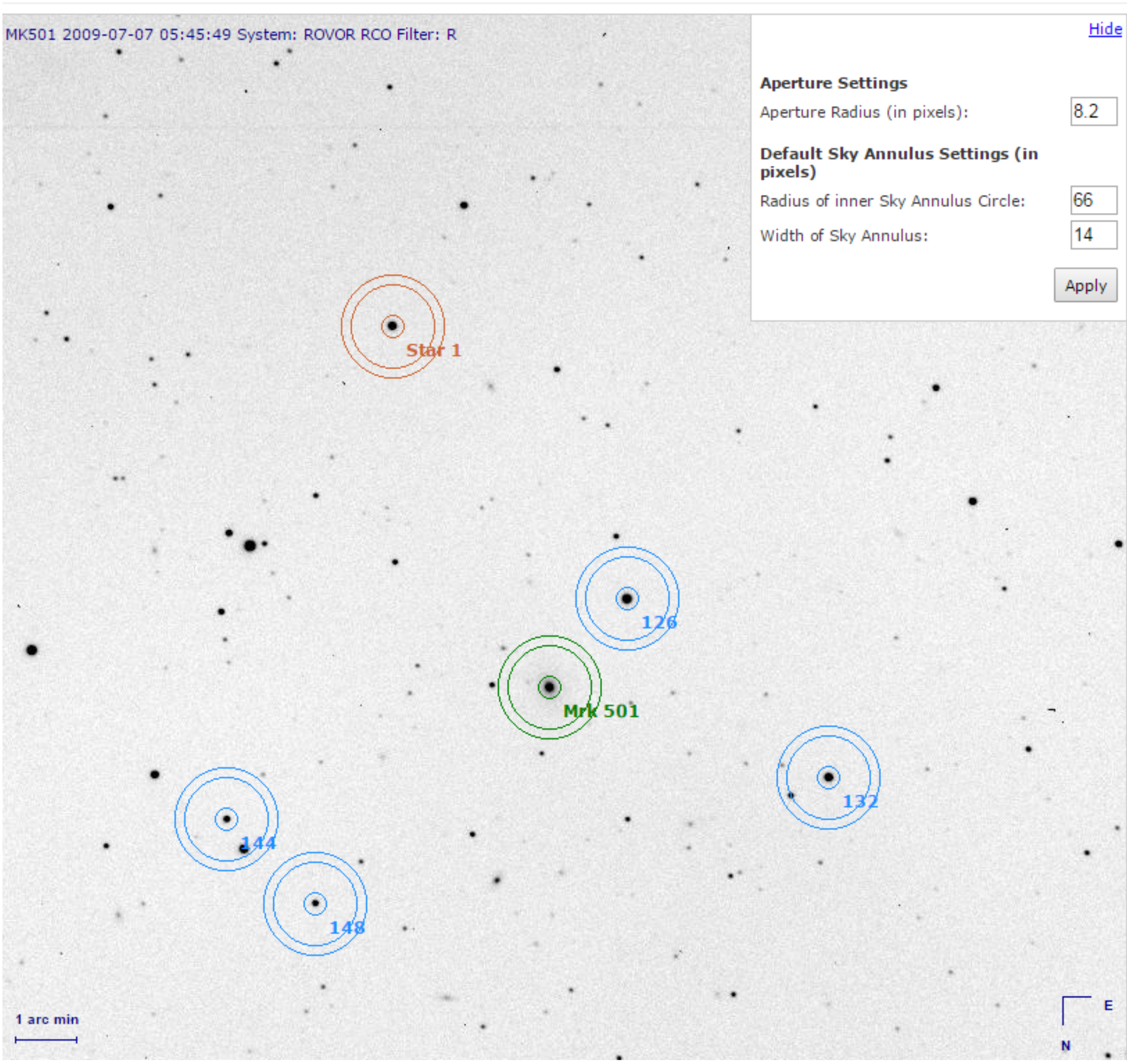

Figure 2.20 ROVOR frame with ensemble stars encircled as shown in *VPhot*. The comparison stars are labeled as "Star 1", "126", "132", "144", and "148". The "Star 1" here is not the same star as the Star 1 from Pace et al. (2012). The Star 1 from Pace et al. (2012) is star 126. In *VPhot* the aperture parameters for 5" is 8.2, 14, and 66 pixels. The 14 pixels refers to the width of the annulus and not the inner radius. (cf. Figure2.19)

Target Star Estimates

Aperture radius: 8.2 Transform Refresh

Target	Mag	Err	Std	Err(SNR)	SNR	Sky	<*
Mrk 501	**13.094**	0.032	0.032	0.005	218	623	
Star 1	**12.766**	0.032	0.032	0.004	280	628	

* - report the target as fainter than the limiting magnitude of 16.568

Image summary

Object:	MK501	Date/Time:	2009-07-07 05:45:49
JD:	2455019.74015	Decimal Date:	2009-07-07.24015
R.A.:	16:53:50.67	Dec:	39:43:13.30
Exp.time:	90 s	Filter:	R
Airmass:	1.0022	Calibration:	F
Telescope:	ROVOR RCO		
Filename:	636060534332596000.fts		

View full FITS header

4 Comparison Stars Toggle Active

Star	IM	SNR	X	Y	Sky	Air	B-V	R-mag	Target estimate	Active
126	-7.783	457	551.706	553.187	619	1.003	0.933	12.124	13.057	✔
132	-7.185	275	697.163	681.739	621	1.003	0.864	12.749	13.084	✔
144	-5.867	91	263.196	711.913	615	1.003	0.620	14.083	13.101	✔
148	-5.635	77	327.158	772.503	619	1.003	0.681	14.348	13.133	✔

Figure 2.21 Table from *VPhot* showing ensemble stars and measured magnitudes in R. The "Mrk 501" row was not used. The "SNR" column shows that the magnitude for star "126" was the most correct. Higher SNR means that telescope picks up more of the signal from the object and less of the background noise. A higher SNR gives more accurate observations. I used the magnitude values from the "Target estimate" column for doing differential photometry in *Mira*.

showing stable magnitudes of the comparison stars. This chart shows that star 126's magnitude is the most accurate, because it has the highest signal-to-noise ratio (SNR) from the ensemble, i.e., 457. Just as with Pace's stable comparison star magnitudes (Pace et al. 2013), *VPhot* has a catalog of comparison stars. The "Target estimate" column shown in Figure 2.21 is the average magnitude of each comparison star. Although only the R filter table is shown, I found the magnitudes for the B and V stars also.

Photing the same frame with different apertures creates an offset in the magnitudes obtained from those apertures. Because there should be a constant offset in magnitude between two different apertures, only rephoting several frames gave me the desired offset. I photed ∼10 nights (in each filter), and with the same ten nights I found the difference between the measured magnitude of the 4 and 1.85 pixels (5”) apertures. After finding these differences I averaged them so that I could find an average offset between the 4 and 1.85 pixels (5”) aperture. These chosen nights and values can be found in the Appendix C; I applied the new shifts to the other 2013 and 2011–2010 data, shifting the light curve up as if observed using a 5” aperture.

$$\overline{\delta_{52}} = \overline{\mu_5 - \mu_2} \tag{2.15}$$

$$\mu_{M_{(5)}} = \mu_{M_{(2)}} + \overline{\delta_{52}} \tag{2.16}$$

The notation above has subscripts "2" and "5” representing the photometry done using the two and five star ensembles, respectively. The two star ensemble was photed using a 4 pixels aperture, while the five star ensemble used a 1.85 pixels aperture. Each was done using 15 and 18 pixels annulus parameters. The average value of the offset between the magnitudes measured by the two apertures is $\overline{\delta_{52}}$, with $\overline{\mu_5 - \mu_2}$ representing the average difference between the aperture magnitudes. In Eq. 2.16, this shift is applied to the individual magnitudes of Mrk 501 (measured using the 4 pixels aperture and two star ensemble) $\mu_{M_{(2)}}$ to find magnitudes $\mu_{M_{(5)}}$ that would have been measured if I had photed all the data using the 1.85 pixels aperture (with the five star ensemble).

Addition of ROVOR Data

Because the ROVOR data only extended to 2013 while WMO’s observations started in 2012 (with two nights in common), it would have been hard to find a pattern from both telescopes. Later data from ROVOR (2014–2016) was discovered and added to the light curve after being photed with the 5” aperture. Once all the data were plotted, a true sinusoidal pattern could be seen, requiring further frequency analysis after removing the offset between the two telescopes.

2.3.3 Shifting ROVOR’s Data to Match WMO’s Data

I aligned the ROVOR data with the WMO data by applying the offset between the two telescopes (dependent on filter type). I was justified in doing this (without affecting the overall result) because Mrk 501 has only one true magnitude at a given time for each filter. If ROVOR and WMO simultaneously observe Mrk 501 using the same filter but get different results, this discrepancy is caused by differences between telescopes and is purely instrumental. The offsets between the telescopes were found by averaging nights when Mrk 501 was both observed by ROVOR and WMO. Only June 5, 2013 and June 14, 2013 fit this criterion. The magnitudes from these two nights are found in Table 2.1.

To calculate the above mentioned offset from ROVOR to WMO, I found the difference between WMO’s and ROVOR’s magnitude in B, R, and V filters for these two nights [Eqs. (2.17) and (2.18)]. I averaged the magnitude differences for the two nights [Eq. (2.19)] to find the average shift between the ROVOR and WMO data. I added the average shift between the two telescopes to their respective observed ROVOR data points so that the ROVOR data were aligned to the WMO data. These steps can be seen below for the B filter:

$$\delta_{\mathrm{Jn5}} = \mu_{\mathrm{Jn5}_{(w)}} - \mu_{\mathrm{Jn5}_{(r)}} \tag{2.17}$$

$$\delta_{\mathrm{Jn14}} = \mu_{\mathrm{Jn14}_{(w)}} - \mu_{\mathrm{Jn14}_{(r)}} \tag{2.18}$$

$$\delta_{wr} = \overline{\delta_{\mathrm{Jn5}} \cup \delta_{\mathrm{Jn14}}} \tag{2.19}$$

$$\rho = \mu_{M_{(r)}} + \delta_{wr} \tag{2.20}$$

Differences between dates and telescopes is notated with δ_x. The two dates in June are represented by the two subscripts Jn5 and Jn14. The subscript (w) means the magnitude was measured using WMO, while (r) is measured by ROVOR. The offset between WMO and ROVOR is given by δ_{wr}. I have introduced ρ meaning the ROVOR data plus δ_{wr}, which are the data points from ROVOR as if measured by WMO. With the ROVOR data matched to WMO, Joe and I were ready for the final frequency analysis.

Table 2.1 Apparent magnitudes of Mrk 501 observed using ROVOR and WMO in R, V, B filters.

B Data			
Date	ROVOR	WMO	Shift
June 5, 2013	14.596	14.714	0.145
June 14, 2013	14.590	14.744	0.154
Average Shift in Telescopes: 0.150 mag			

V Data			
Date	ROVOR	WMO	Shift
June 5, 2013	13.985	14.076	0.091
June 14, 2013	14.012	14.083	0.070
Average Shift in Telescopes: 0.081 mag			

R Data			
Date	ROVOR	WMO	Shift
June 5, 2013	13.399	13.574	0.175
June 14, 2013	13.389	13.576	0.187
Average Shift in Telescopes: 0.181 mag			

2.4 Frequency Analysis in *Period04*

We employed a different frequency analysis program, *Period04* (https://www.univie.ac.at/tops/*Period04*/), to find periods in the total data set. *Period04* allows for the user to specify the number of frequencies sought for in a data set—we had it search for four. It returned values for the amplitude of the curve, phase shift, and the frequency of each fit. The fits took the form of a sine-series expansion:

$$y_i(t) = Z + \sum_{i=1}^{4} A_i \times \sin(2\pi f_i t + \phi_i) \tag{2.21}$$

The symbol $y_i(t)$ represents the value, at time t (value of JD), of a given point on the fit function corresponding to the i-th frequency; Z is the y-offset from zero; A_i represents the amplitude of the sinusoid (depending on the frequency index i); f_i refers to the i-th frequency found in the data set (when inverted it is the resulting period, in days); and ϕ_i is the phase shift of the fit function, corresponding to the i-th frequency. I refer to these five values as fit parameters. This function was used to find the period fits for each filter. *Period04* returned a total of 12 values per parameter (except for Z, which only had one for each filter), one for each corresponding frequency in a given filter, as shown in Table 2.2. We used the sinusoidal fit (for a given filter) with the longest period and subtracted it from the light curve data points of the given filter, yielding the first residual graph for a given filter. Next, we took this value and subtracted the next longest period, obtaining a second residual. This process was repeated for each of the the different sinusoidal fits so that we ended with three residuals. Residuals are more fully explained in Chapter 3.

Table 2.2 Values returned from *Period04* for the y-offset, amplitude, frequency, and phase shift.

R Data Z_R = 13.3406 mag

i	Frequency [$days^{-1}$]	Amplitude [mag]	Phase Shift [rad]
1	0.00043336726587531	0.0576643772519742	0.881946969699972
2	0.00840459775921598	0.0111716749210405	0.180599284892712
3	0.00459969683275247	0.0152652554239398	0.187995727363652
4	0.0149545130751802	0.0062759744758767	0.648866746628151

V Data Z_V = 13.8644 mag

i	Frequency [days^{-1}]	Amplitude [mag]	Phase Shift [rad]
1	0.00043336726587531	0.0624060576627904	0.882204006592988
2	0.00840459775921598	0.0211686082485394	0.0898502299227069
3	0.00459969683275247	0.0258009238243735	0.18381606562268
4	0.0149545130751802	0.0106781103080168	0.60100662620909

B Data Z_B = 14.5753 mag

i	Frequency [$days^{-1}$]	Amplitude [mag]	Phase Shift [rad]
1	0.00043336726587531	0.0990588257	0.863771
2	0.00840459775921598	0.0264912927	0.406085
3	0.00459969683275247	0.0271839978	0.956241
4	0.0149545130751802	0.0172542086	0.592777

Chapter 3

Results

I began this thesis by explaining what Mrk 501 is and why it is important. Research efforts for observing Mrk 501 in a variety of wavelengths were presented, as well as work previously done at BYU. Different photometry programs, *VPhot* and *Mira*, were discussed and the process of extracting the data from frames was laid out. After data were used to make a light curve, we performed frequency analysis to find periods in the brightness variations of Mrk 501. In this concluding chapter, I present the long-term, optical-wavelength period of $\sim$2300 days. Shorter possible wavelengths and their actuality is decided. Different approaches to further research on Mrk 501 are suggested.

3.1 Periodicity of Markarian 501 and Residuals

Using MATLAB, I plotted the B, V, and R filter light curves with the longest period fit as illustrated in Figure 3.1 (MATLAB code can be found in Appendix D). This long-term period, extending 2307 days, is apparent in each of the three filters. For neatness, the data from R and B filters have been shifted by a few tenths of a magnitude, closer to V. It is important to point out that the spread of magnitudes varied from filter to filter. The B filter had the largest variation in magnitude because of the higher energy observed; with V filter variations, smaller; and R filter, smallest. This is expected, as discussed in Section 1.3, because higher energy has higher variation. The duration for observing Mrk 501 was long enough for us find this long-term period. This apparent sinusoidal pattern of magnitude is inherent to Mrk 501 during this time frame because the amplitude is too large be the result of any noise.

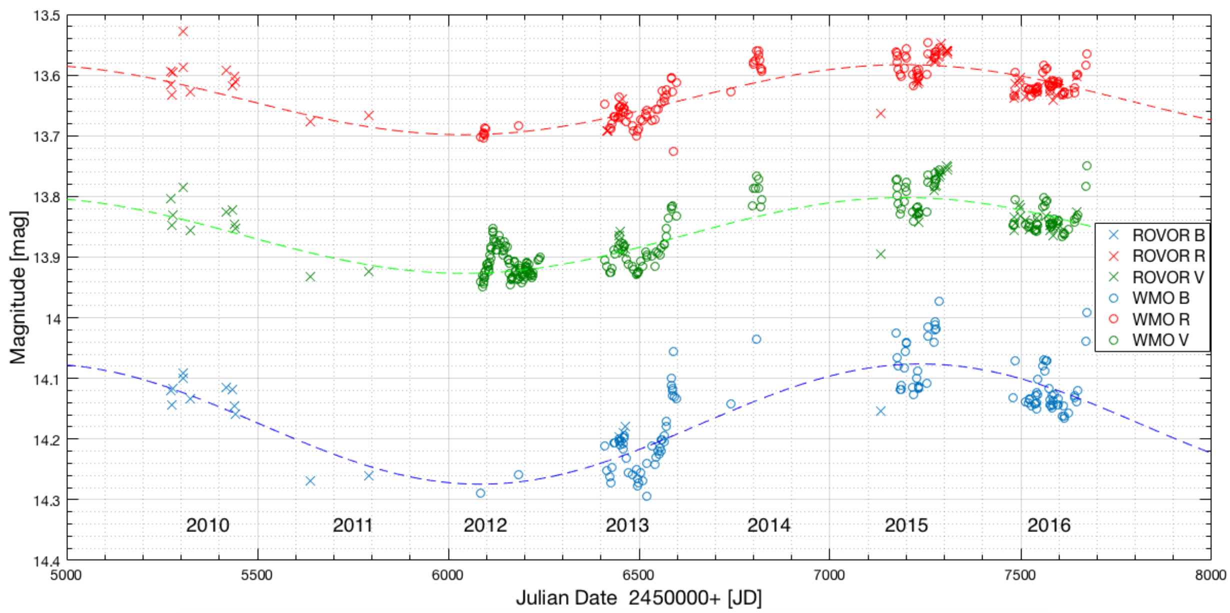

Figure 3.1 ROVOR (X's) and WMO (◯'s) data in B (blue), V (green), and R (red) filters plotted vs Julian Date along with respective sinusoidal fits from *Period04* (added to exhibit oscillations). The light curve extends from 2010 to 2016 with ROVOR and WMO data woven together. The March 2010–June 2013 data are taken from ROVOR, July 2012–September 2015 from WMO, with later ROVOR data from October 2015–September 2016. The data from ROVOR are represented by X's and WMO, ◯'s. This is a reverse log-scale graph, therefore brighter observations are closer to zero (higher on the graph). In this graph, for appearance, the average magnitude from the B filter were shifted down from 14.6 by 0.4 mag, while R was shifted up from 13.3 by 0.3 mag. The overall periodicity in the light curve is emphasized by the dotted sinusoid fits, extending 2307 days. In this light curve, around 2456500 JD in each filter, a smaller period was seen. The data for this graph can be found in Appendix E. This existence of a smaller oscillation shows evidence for binary black hole, discussed in Rivest (2017, Brigham Young University).

After plotting the longest period in the light curve, I also made graphs of residuals in MATLAB

(Appendix D), in hope of finding other real periods in Mrk 501. The first residuals were found by subtracting the longest period (dashed sinusoid) from the observed magnitudes in B (in blue), V (in green), and R (in red) filters. The next residuals were created by subtracting off the second longest period from the first residual curve, this process was repeated to obtain each next set of residuals.

The residuals (represented with dots) plotted with corresponding periods (represented with solid lines), of 119 and 217 days, are shown in Figure 3.2. Each column of figures represent a period, while the rows (descending) show R (in red), V (in green), and B (in blue) filters. The V filter residuals, in the second row and first column of Figure 3.2, show high accuracy for periods fitting the residuals around 2456200 JD. Because of the accuracy between the residuals and fit at this time in every filter, the 119-day period is a real period found in Mrk 501, but it cannot have a perfect fit.

Using residuals allowed me to determine the relative accuracy for the proposed periods from *Period04*. The better the periods fit the residuals, the greater the possibility that the period corresponding to that residual is real. Real periods are those that are from Mrk 501, itself, and are not a result of noise, which could cause false sinusoidal patterns. This method of finding possible periods, visually, by comparing the them against residuals is only accurate for the first few periods. In *Period04*, when requesting to find periods, every new period that is returned is significantly smaller in magnitude, so that after a few periods the amplitude of the sinusoid is on the same order of magnitude as potential noise. Only the two residuals were plotted with their corresponding sine fits. One more could have been plotted, but the actual signal for the fourth period was most likely noise.

The light curve contains a long-term sinusoidal pattern, therefore the brightness of Mrk 501 fluctuates with time from a maximum to minimum magnitude. This sinusoidal pattern is also seen in an eclipsing binary supermassive black hole (SMBH) system. As one SMBH eclipses the

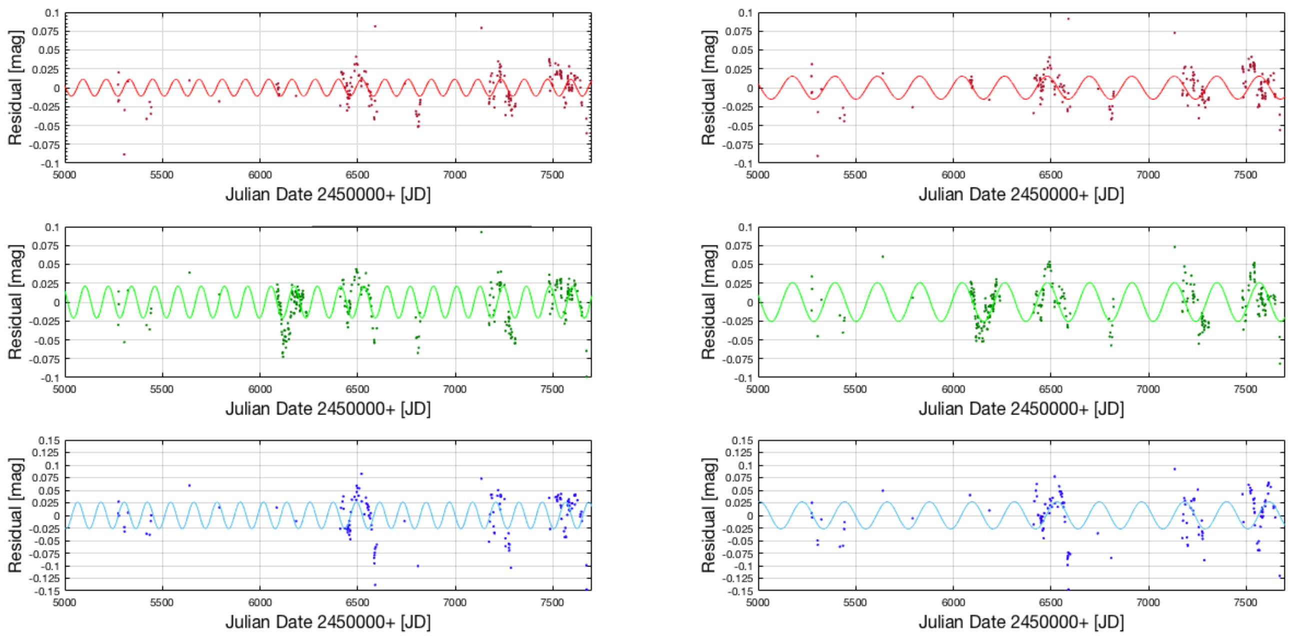

Figure 3.2 The two smaller periods and their respective residuals in R (red), V (green), and B (blue) filters (descending). The magnitude difference (ranging -0.1–0.1 mag for V and R and -1.5–1.5 mag for B) is plotted against Julian Date extending from 2455000–2457475 JD. The residual points are represented by ·'s and the period fits are shown by solid lines. The top row shows the R filter residuals; middle, V; and bottom, B—each with the 119-day period on the left-hand column and 217-day period on the right. The clearest and most accurate fit between residuals and their corresponding periods happens in the V filters around 2456200. The 119-day period has the better fit out of the two, and because it fits so well, Joe and I concluded that there is 119-day period in Mrk 501. The 217-day period is not as good of a fit, so we are not as confident that this period is real. The residual values are available in Appendix F.

other, a fluctuation in magnitude would be detected, comparable to the pattern seen in Figure 3.1. Although not conclusive, we have provided further evidence the possibility that Mrk 501 contains a binary SMBH system. The other two periods of 119 and 217 days, in Figure 3.2, support evidence for multiple black holes, however, our confidence level for these periods is lower than that for the longer period of 2307 days. More data needs to be taken to verify these conclusions.

3.2 Further Work

3.2.1 Missing 2009 Data

The 2009 data were not used in the final light curve. After seeing a seemingly random drop in the brightness for data around May 2009–June 2009, I was not confident in using the photing parameters found in Section 2.2.4. I later learned that the coupled charged device (CCD) for ROVOR was changed in May 2009. This older CCD had a different plate-scale than the current CCD in ROVOR, and therefore needed different parameters.

The May 2009 flare is another plausible reason for the drop in magnitude. This flare was recorded at gamma ray wavelengths (Neronov et al. 2012), enduring for a month. The 2009–2013 light curve (Figure 2.15) showed the 2009 data decreasing in magnitude below other later years. I was unable to determine whether the recorded gamma ray burst effected the drop in magnitude. It is possible that this flare could have affected the optical wavelength observations, which could shed light on why these nights (May 2009) are at a minimum magnitude.

Because of these reasons, i.e., the change in CCD and possible flaring, the 2009 data were not included in the light curve. These two events made it difficult from me to understand why the brightness dropped, as it could be from either event, neither of them, or the combination of both events. After understanding effects of the 2009 flare and finding appropriate parameters for the old CCD on *Mira*, I invite future BYU students to rephot the 2009 data. This would allow the 2009 data to be included in our light curve and verify the 2307-day period found.

3.2.2 Correlation in Wavelengths

In addition to the optical wavelength observations, as described in Section 1.3, Mrk 501 has also been observed at various other wavelengths. These other observations could be included in the creation of a more comprehensive light curve. Piecing together a more integrated light curve would add to the evidence for MBHS's. Observations among different wavelengths, during similar time frames, could be analyzed in search of correlations between energy levels. Such an analysis would shed more light on how energy levels interact together and explain why the 2009 data dim (Section 3.2.1).

3.2.3 Improved Nightly Average

The nightly averages in Mrk 501 could have been found using more accurate methods. In order to find the average magnitude per a given night, I used *Excel*'s AVG function and averaged the apparent magnitude for each frame. This method was an accurate average if each night had the same number of frames and they were evenly spaced during the observation period. Unfortunately, this was not the case. Some nights had few frames, while others contained hundreds. The differences in the number of frames per night effected bias AJD values, shifting the average magnitude closer to the time of night with the most frames. If a night had observations in which most of the frames were taken at the beginning of the night, then the AJD for that night would resemble the beginning of the night. To find more exact nightly averages in magnitude, and hence assemble a more accurate light curve, I recommend using more advanced statistics that take into account differing in the number of frames and inconsistent spacing between subsequent observations.

3.2.4 Longer Observations

Although the 2307-day period may seem long, with prolonged observations, finding even longer periods is possible. Mrk 501 has only been observed for seven years in BYU telescopes. Further observations are the key to understanding the time-dependent evolution of Mrk 501's light curve. For example, Bon et al. (2016), after 43 years of optical observations, found a long-term period of $\sim$5700 days in NGC 5548 (another AGN). Every addition to our light curve will contribute to the understanding of Mrk 501's photometric behavior.

3.3 Conclusion

In this project, the data consisted of all B, V, and R calibrated observations taken by ROVOR and WMO, extending March 2010–September 2016. Differential photometry was performed using five stable comparison stars and a 5” aperture. ROVOR’s frames were photed using *Mira* and WMO’s frames using *VPhot*. The light curve shows an apparent 2307-day period in Mrk 501’s optical brightness, along with two shorter periods of 119 and 217 days. The long-term period provides evidence for a binary black hole system [cf. Rivest (2017, Brigham Young University)]. There appears to be a 119-day period in the brightness variations of Mrk 501. However, due to possible noise, we are less certain of the 217-day period. The 2009 data should added to the light curve after photing with more accurate photometric parameters and taking the old CCD and 2009 flare into account. Continual monitoring, combining of light curves, and employing of advanced statistics are needed to increase confidence of this possible MBHS and discovered periods therein.

Appendix A

Equation Notation

I invented an unorthodox way to represent values that I used throughout my research. I feel that my notation is both clear and simplified, and an alternative to overly using subscripts. Some of the symbols chosen are nowhere intuitive. I created this notation for this thesis to describe the manipulation of values to allow the reader more insight, as only describing the equations in words would be repetitively long and complex in understanding. Below I have included a table to reference that lays out symbols used in equations.

δ: used to represent a magnitude difference or offset. Usually two subscripts are associated with this variable, but when describing a difference between magnitudes of a same date only one subscript is needed. Thus the difference between magnitude of a and b is δ_{ab} and the magnitude difference between ROVOR and WMO on the same date is δ_{date}.

μ: used to represent the magnitude of either Mrk 501 or a specific star. μ_a would be used to represent the magnitude of a.

C: used to represent the amount needed to shift the data of the flipped frame.

B, V**,** R**, and** I**:** used to represent the all apparent magnitudes of Mrk 501 in a given filter or to specify in which filter the observations were observed.

ρ**:** a variable representing shifting all the ROVOR data by the offset from WMO to remove the offset from the telescopes so that frequency analysis can be performed.

M **,** 1**, and** 4**:** subscript for Mrk 501, Star 1, and Star 4.

Jn5 and Jn14: subscript for June 5 and June 14, 2013.

N**:** represents the number of photon flux counts of an object. Where N_a would represent the number of counts measured from a on a given frame.

2 **and** 5**:** represents the two and five star ensemble. When used as subscripts they mean that the measurement was done using the aperture sizes corresponding to the ensemble. For the two star ensemble the aperture radius was 4 pixels and for the five star a 1.85 pixels (5”) aperture was used.

r**:** used to specify that the measurements were done using the ROVOR frames.

w**:** used to specify that the measurements were done using the WMO frames.

(u) **and** (f)**:** used to specify that the values are from the upright (u) or the flipped (f) frames.

Z**:** the value needed to shift the period fit to match the data.

A_i**:** the amplitude of the sine function of the i-th frequency before adding the Z shift.

f_i**:** the i-th frequency for the sine fit.

ϕ_i: the phase shift of the sine fit of the i-th frequency.

average [$\overline{abc}$] : is placed over a variable to specify that the average is to be taken. The average that is referred to is the same as *Excel*'s "AVG" function over the nightly values with variable "abc". When taking an average over more than one different set of numbers combined, the $\cup$ symbol is used. For example, if I wanted to know the average magnitude in all the filters together, I would write: $\overline{B \cup V \cup R \cup I}$.

referenced by:$Y_{z_{(x)}}$ To be more clear in explaining what filter, telescope, and aperture that was used I made the reference notation. When a single variable is surround by parentheses in the second subscript [( )], the frame of reference is given by the variable. Whether a measurement was taken from a flipped or unflipped frame is given by (f) and (u). Measurements made by ROVOR are notated (r) and WMO, (w). Frames that have been photed using the 4 pixels aperture are notated with (3) and the 5” aperture is a (5) as the second subscript. After all the data have the offset removed from them, each filter has a (V) second subscript, showing that these are the values that the V filter would have recorded. I got this idea from relativity and how each observer has a different frame of reference.

Table A.1 Notation of Equations

Symbols

Symbol	Equations
δ	offset
μ	magnitude
C	correction to be added to the flipped frames
B	B filter magnitudes of each night
V	V filter magnitudes of each night
R	of R filter magnitudes of each night

I	of I filter magnitudes of each night
ρ	ROVOR data with added shift from WMO
$y_i(t)$	the value of the i-th sine fit function at time t
Z	offset from zero
A_i	amplitude of i-th frequency sine fit function
f_i	i-th frequency of sine fit
t	time in JD
ϕ_i	phase shift of i-th frequency

1st Subscripts

1st Subscript	Represents
M	Mrk 501
1	Star 1
4	Star 4
Jn5	June 5, 2013
Jn14	June 14, 2013
N	number of counts
B	of B filter
V	of V filter
R	of R filter
I	of I filter
2	from two star ensemble (4 pixels aperture)
5	from five star ensemble (1.85 pixels aperture)
w	WMO
r	ROVOR

i	index corresponding to a given frequency found by *Period04*

2nd Subscripts

2nd Subscript	as measured in
(u)	upright frame
(f)	flipped frame
(r)	ROVOR
(w)	WMO
(2)	4 pixels aperture (two star ensemble)
(5)	5” aperture (five star ensemble)
(V)	the V filter

Appendix B

2009–2013 B, V, R, and I Filter data

Table B.1 Data Corresponding to Fig. 2.15

Gregorian Date	Julian Date [JD]	Filter Type	$\mu_M[mag]$	σ_M (stdev) [mag]	σ_{14} (stdev) [mag]
16-May-09	2454967.789	B	14.48667857	0.014982974	0.03723552
17-May-09	2454968.787	B	14.44705	0.040698366	0.05912133
18-May-09	2454969.791	B	14.47348667	0.013960499	0.03052984
28-May-09	2454979.701	B	14.43184	0.016086054	0.12793887
30-Jun-09	2455012.887	B	14.40972857	0.006567271	0.04439215
7-Jul-09	2455019.856	B	14.39245	0.032346181	0.0633382
10-Jul-09	2455022.783	B	14.35732	0.012378622	0.03473734
17-Jul-09	2455029.859	B	14.38013	0.014228145	0.01905138
28-Jul-09	2455040.837	B	14.387775	0.013470258	0.03586992
29-Jul-09	2455041.816	B	14.3883375	0.010815721	0.03035783
18-Aug-09	2455061.685	B	14.32259	0.009214174	0.02923244
19-Aug-09	2455062.763	B	14.3191375	0.009773278	0.02708415
21-Aug-09	2455064.763	B	14.3334375	0.010130426	0.18986623

22-Aug-09	2455065.762	B	14.3426625	0.015476705	0.04604624
26-Aug-09	2455069.783	B	14.32692857	0.014396494	0.02875708
27-Aug-09	2455070.741	B	14.3347875	0.008115846	0.02850063
1-Sep-09	2455075.717	B	14.32715833	0.015930281	0.06882959
12-Sep-09	2455086.75	B	14.397425	0.013660009	0.03617232
21-Sep-09	2455095.736	B	14.401875	0.011026445	0.01435676
23-Sep-09	2455097.71	B	14.3797	0.013085616	0.04563168
24-Sep-09	2455098.718	B	14.38638	0.009689788	0.01803419
25-Sep-09	2455099.708	B	14.38681667	0.009379001	0.00909278
26-Sep-09	2455100.661	B	14.38398333	0.015906152	0.06201721
18-Mar-10	2455273.85	B	14.30255	0.011923786	0.04057729
20-Mar-10	2455276.031	B	14.32634305	0.010347625	0.04907292
21-Mar-10	2455276.99	B	14.29864	0.005803706	0.01731127
18-Apr-10	2455304.957	B	14.28225	0.078775821	0.04161186
19-Apr-10	2455305.864	B	14.273675	0.003413088	0.00385184
7-May-10	2455323.784	B	14.31536667	0.008738612	0.02342847
10-Aug-10	2455418.685	B	14.2973	0.001442221	0.01070389
26-Aug-10	2455434.689	B	14.29945	0.030759145	0.06307392
1-Sep-10	2455440.658	B	14.32815	0.009545942	0.0496389
3-Sep-10	2455442.656	B	14.34015	0.000494975	0.01244508
18-Mar-11	2455638.981	B	14.451475	0.020035697	0.09045004
18-Aug-11	2455791.687	B	14.4425	0.01046518	0.14948237
5-Jun-13	2456448.725	B	14.37727083	0.011619192	0.03464681
7-Jun-13	2456450.737	B	14.387088	0.012261094	0.03981314
14-Jun-13	2456457.848	B	14.37051	0.016479775	0.04400494

19-Jun-13	2456462.841	B	14.36071338	0.033824107	0.04125266
10-May-09	2454961.837	V	13.62037273	0.020449161	0.08582608
16-May-09	2454967.794	V	13.61344667	0.008381431	0.0170776
17-May-09	2454968.792	V	13.55354667	0.042583865	0.04471995
18-May-09	2454969.795	V	13.60422	0.008268028	0.03808982
28-May-09	2454979.706	V	13.57514286	0.010825235	0.06164058
30-Jun-09	2455012.888	V	13.56592857	0.007387538	0.02721537
7-Jul-09	2455019.856	V	13.55534444	0.015196802	0.05168437
10-Jul-09	2455022.772	V	13.53894	0.007044714	0.03420421
17-Jul-09	2455029.859	V	13.5437	0.016794444	0.02464187
28-Jul-09	2455040.836	V	13.553275	0.007374037	0.07742539
29-Jul-09	2455041.816	V	13.5474	0.010847119	0.01829036
18-Aug-09	2455061.779	V	13.49879	0.014714577	0.01342106
19-Aug-09	2455062.763	V	13.5016	0.009124379	0.02197139
21-Aug-09	2455064.763	V	13.5085125	0.010742497	0.00801494
22-Aug-09	2455065.762	V	13.5211	0.037117612	0.02701046
26-Aug-09	2455069.773	V	13.50345	0.014874427	0.0122939
27-Aug-09	2455070.741	V	13.5134375	0.006386132	0.02007095
1-Sep-09	2455075.717	V	13.50821667	0.014804954	0.04556409
12-Sep-09	2455086.75	V	13.5446	0.009379055	0.02601461
21-Sep-09	2455095.736	V	13.54695	0.006888396	0.02591293
23-Sep-09	2455097.71	V	13.541225	0.008785357	0.04149165
24-Sep-09	2455098.709	V	13.54025	0.003005162	0.01143398
25-Sep-09	2455099.708	V	13.54351667	0.005343189	0.02118556
26-Sep-09	2455100.661	V	13.54576667	0.006446291	0.03690803

18-Mar-10	2455273.854	V	13.4785	none	
20-Mar-10	2455275.946	V	13.52297647	0.009297452	0.02073261
21-Mar-10	2455276.999	V	13.50623333	0.008326063	0.01137776
18-Apr-10	2455304.962	V	13.4603	0.003959798	0.03747666
7-May-10	2455323.876	V	13.53174029	0.008683675	0.03959798
10-Aug-10	2455418.687	V	13.50133333	0.00595007	0.03066094
26-Aug-10	2455434.691	V	13.4983	0.009899495	0.05642712
1-Sep-10	2455440.659	V	13.5211	0.004949747	0.02149605
3-Sep-10	2455442.657	V	13.5272	0.002969848	0.01103087
18-Mar-11	2455638.983	V	13.6072	0.009201811	0.0355038
18-Aug-11	2455791.702	V	13.5982	0.024693503	0.10965364
5-Jun-13	2456448.701	V	13.540136	0.014617338	0.02980877
7-Jun-13	2456450.714	V	13.53364091	0.033297771	0.10179942
14-Jun-13	2456457.745	V	13.56783	0.009141	0.03186865
19-Jun-13	2456462.839	V	13.562428	0.005461038	0.02142484
10-May-09	2454961.671	R	13.05745405	0.034550483	0.09923281
14-May-09	2454965.797	R	13.07692	0.005577781	0.01971531
15-May-09	2454966.826	R	13.07232444	0.005055922	0.01979161
16-May-09	2454967.791	R	13.07994943	0.006173798	0.01734327
17-May-09	2454968.836	R	13.06137157	0.027596256	0
18-May-09	2454969.826	R	13.06218324	0.00984857	0.02306655
28-May-09	2454979.827	R	13.03370181	0.012757224	0.05896303
30-Jun-09	2455012.877	R	13.02995	0.006215878	0.02852327
6-Jul-09	2455018.865	R	13.01267347	0.008539907	0.03566375
7-Jul-09	2455019.802	R	13.02586633	0.017473263	0.04067105

10-Jul-09	2455022.876	R	13.0089855	0.00989054	0.03264316
17-Jul-09	2455029.859	R	13.00244	0.010906491	0.02516453
28-Jul-09	2455040.837	R	13.01105	0.006253913	0.01902082
29-Jul-09	2455041.816	R	13.01025	0.015310967	0.01587071
30-Jul-09	2455042.865	R	13.0138875	0.007942791	0.0167252
31-Jul-09	2455043.863	R	13.00794127	0.010191594	0.01681404
3-Aug-09	2455046.816	R	13.00343373	0.01168436	0.02859331
11-Aug-09	2455054.816	R	12.97304884	0.007063635	0.02525294
18-Aug-09	2455061.779	R	12.96805	0.014437855	0.01737457
19-Aug-09	2455062.763	R	12.9708375	0.009675143	0.01862853
21-Aug-09	2455064.763	R	12.9749	0.013098528	0.01862801
22-Aug-09	2455065.762	R	12.9770625	0.009061526	0.02542573
26-Aug-09	2455069.773	R	12.9684625	0.011124354	0.00776218
27-Aug-09	2455070.741	R	12.981675	0.00875977	0.01772262
1-Sep-09	2455075.717	R	12.989075	0.004617853	0.0270141
12-Sep-09	2455086.75	R	13.028975	0.022278745	0.00939415
21-Sep-09	2455095.736	R	13.0133	0.012269203	0.01189342
23-Sep-09	2455097.71	R	12.9944	0.007933473	0.03559981
24-Sep-09	2455098.709	R	13.00023333	0.013067925	0.01345952
25-Sep-09	2455099.708	R	12.99816667	0.007836241	0.01404151
26-Sep-09	2455099.708	R	13.00478333	0.009671694	0.03390027
9-Nov-09	2455143.645	R	12.99961429	0.033707504	0.04476314
17-Mar-10	2455272.843	R	12.99277143	0.010697694	0.07423586
18-Mar-10	2455273.863	R	12.9707	0.00903899	0.06326204
20-Mar-10	2455275.935	R	13.0094	0.00670775	0.00963874

21-Mar-10	2455277.004	R	12.97283333	0.004966219	0.0125108
18-Apr-10	2455304.939	R	12.90486485	0.013942642	0.09349897
19-Apr-10	2455305.982	R	12.96369167	0.007020031	0.01455875
7-May-10	2455323.878	R	13.00430692	0.000980166	0.08428713
10-Aug-10	2455418.688	R	12.969	0.001835756	0.00660101
26-Aug-10	2455434.693	R	12.9938	0.005374012	0.00848528
1-Sep-10	2455440.661	R	12.9792	0.009192388	0.00141421
3-Sep-10	2455442.659	R	12.98825	0.000777817	0.00636396
18-Mar-11	2455638.985	R	13.053425	0.009164924	0.03142287
18-Aug-11	2455791.712	R	13.04426667	0.00791906	0.03687254
3-May-13	2456415.974	R	13.06809565	0.006847725	0.02696632
4-May-13	2456416.929	R	13.06848492	0.005608317	0.02696632
31-May-13	2456443.892	R	13.04989167	0.007236141	0.0207851
2-Jun-13	2456445.797	R	13.04621814	0.006647246	0.02204212
4-Jun-13	2456447.811	R	13.02163282	0.012951337	0.02847188
5-Jun-13	2456448.832	R	13.0383696	0.006536019	0.02173174
7-Jun-13	2456450.841	R	13.03397996	0.0090431	0.02456207
11-Jun-13	2456454.885	R	13.01638176	0.015346933	0.10179942
14-Jun-13	2456457.85	R	13.027896	0.007080812	0.03222033
19-Jun-13	2456462.839	R	13.047428	0.005461038	0.02142484
30-Jun-09	2455012.877	I	12.377275	0.007126961	0.02002425
17-Jul-09	2455029.859	I	12.36261	0.009737836	0.05671088
28-Jul-09	2455040.837	I	12.360175	0.010965498	0.01995881
29-Jul-09	2455041.816	I	12.3701375	0.007469354	0.04074148
18-Aug-09	2455061.779	I	12.33296	0.006315272	0.03158171

19-Aug-09	2455062.763	I	12.3381	0.010742173	0.06186676
21-Aug-09	2455064.763	I	12.33445	0.009278855	0.03205526
22-Aug-09	2455065.762	I	12.32655	0.016774981	0.04452438
26-Aug-09	2455069.761	I	12.33428571	0.007103621	0.03156049
27-Aug-09	2455070.741	I	12.3405	0.008758343	0.03676831
12-Sep-09	2455086.75	I	12.36685	0.0057181	0.01721627
21-Sep-09	2455095.736	I	12.363025	0.005324394	0.05907901
23-Sep-09	2455097.71	I	12.35345	0.00847919	0.0157297
24-Sep-09	2455098.709	I	12.35565	0.008367736	0.03878261
25-Sep-09	2455099.708	I	12.35651667	0.015546757	0.06276237
26-Sep-09	2455100.661	I	12.34778333	0.023627731	0.05502896
20-Mar-10	2455275.939	I	12.367675	0.005679731	0.01737625
21-Mar-10	2455277.006	I	12.3461	0.002406242	0.0125108
10-Aug-10	2455418.69	I	12.31266667	0.001101514	0.01074058
26-Aug-10	2455434.694	I	12.3509	0.000424264	0.01810193
1-Sep-10	2455440.663	I	12.3469	0.012020815	0.02333452
3-Sep-10	2455442.66	I	12.33155	0.001484924	0.0019799
18-Mar-11	2455638.986	I	0.004972843	0.004972843	0.04719898

Appendix C

Converting 4 Pixels Aperture to 5" Tables

Table C.1
B Data Converting 4 Pixels Aperture to 5"

aperture	AJD [JD]	4 pixels	1.85 (5") pixels	difference
3/18/2010	2455273.85	14.30255	14.54345	0.2409
3/21/2010	2455276.99	14.29864	14.53918	0.24054
4/18/2010	2455304.957	14.28225	14.47655	0.1943
4/19/2010	2455305.864	14.27368	14.4869	0.213225
5/7/2010	2455323.784	14.31537	14.5469	0.231533
8/10/2010	2455418.685	14.2973	14.51467	0.217367
8/26/2010	2455434.689	14.29945	14.5097	0.21025
9/1/2010	2455440.658	14.32815	14.52945	0.2013
9/3/2010	2455442.656	14.34015	14.5336	0.19345
3/18/2011	2455638.981	14.45148	14.71178	0.2603
8/18/2011	2455791.687	14.4425	14.67625	0.23375

6/5/2013	2456448.725	14.37727	14.57741	0.200138
6/7/2013	2456450.737	14.38709	14.59776	0.210676
$\overline{\delta_{52}}$ (B): 0.219056038 mag				

Table C.2
V Data Converting 4 Pixels Aperture to 5”

aperture	AJD [JD]	4 pixels	AJD [JD]	1.85 (5”) pixels	δ_{52}
3/18/2010	2455273.85	13.4785	2455273.85	13.9493	0.4708
3/20/2010	2455276.04	13.52506	2455275.93	13.98283	0.457764
3/21/2010	2455277	13.50623	2455277	13.9645	0.458267
4/18/2010	2455304.96	13.4603	2455304.96	13.94523	0.484925
5/7/2010	2455323.88	13.53174	2455323.79	13.9767	0.44496
8/10/2010	2455418.69	13.50133	2455418.69	13.9659	0.464567
8/26/2010	2455434.69	13.4983	2455434.69	13.92895	0.43065
9/1/2010	2455440.66	13.5211	2455440.66	13.93605	0.41495
9/3/2010	2455442.66	13.5272	2455442.66	13.98775	0.46055
3/18/2011	2455638.98	13.6072	2455638.98	14.08148	0.474275
8/18/2011	2455791.7	13.5982	2455791.7	14.01652	0.418317
6/5/2013	2456448.7	13.54014	2456448.7	13.96861	0.428476
6/7/2013	2456450.71	13.53364	2456450.71	13.96786	0.434223
6/14/2013	2456457.74	13.56783	2456457.74	13.99038	0.42255
6/19/2013	2456462.84	13.56243	2456462.73	13.9647	0.402272
$\overline{\delta_{52}}$ (V): 0.444503 mag					

Table C.3
R Data Converting 4 Pixels Aperture to 5”

aperture	AJD [JD]	4 pixels	AJD [JD]	1.85 (5”) pixels	δ_{52}
5/3/2013	2456415.974	13.0681	2456415.972	13.38493	0.316834
5/4/2013	2456416.929	13.06688	2456416.947	13.41296	0.346078
5/31/2013	2456443.892	13.04989	2456443.892	13.37048	0.32059
6/2/2013	2456445.744	13.04777	2456445.911	13.37409	0.326323
6/4/2013	2456447.898	13.01508	2456447.899	13.40385	0.388767
6/5/2013	2456448.927	13.03717	2456448.927	13.37137	0.3342
6/7/2013	2456450.887	13.03885	2456450.886	13.37325	0.334408
6/11/2013	2456454.885	13.01638	2456454.89	13.33986	0.323479
6/14/2013	2456457.85	13.0279	2456457.849	13.38032	0.35242
6/19/2013	2456462.839	13.04743	2456462.839	13.35452	0.307088
3/18/2011	2455638.985	13.05343	2455638.985	13.46195	0.408525
8/18/2011	2455791.712	13.04427	2455791.712	13.40928	0.365017
9/1/2010	2455440.661	12.9792	2455440.661	13.3274	0.3482
9/3/2010	2455442.659	12.98825	2455442.659	13.4078	0.41955
5/7/2010	2455323.878	13.005	2455323.789	13.3702	0.3652
8/10/2010	2455418.688	12.969	2455418.688	13.3648	0.3958
3/17/2010	2455272.843	12.99277	2455272.843	13.35816	0.365386
4/18/2010	2455304.936	12.90343	2455304.936	13.32563	0.422205
3/18/2010	2455273.863	12.9707	2455273.863	13.36085	0.39015
4/19/2010	2455305.982	12.96369	2455305.982	13.33862	0.374925
3/20/2010	2455275.935	13.0094	2455275.935	13.38144	0.372042

3/21/2010	2455277.004	12.97283	2455277.004	13.3647	0.391867
8/26/2010	2455434.693	12.9938	2455434.693	13.32115	0.32735
$\overline{\delta_{52}}$(R): 0.360713 mag					

Appendix D

MATLAB Code

```
clear; close all;

%time and date for rovor B values
xbrovor=dlmread('B5asrovor.txt','\t','A1..A17');
ybrovor=dlmread('B5asrovor.txt','\t','B1..B17')-.4-.0264;

%time and date for rovor R values
xrrovor=dlmread('R5asrovor.txt','\t','A1..A61');
yrrovor=dlmread('R5asrovor.txt','\t','B1..B61')+.3;

%time and date for rovor V values
xvrovor=dlmread('V5asrovor.txt','\t','A1..A53');
yvrovor=dlmread('V5asrovor.txt','\t','B1..B53');

%time and date for WMO B values
```

```
xbwmo=dlmread('newaveBwmo121.txt','\t','A1..A121');
ybwmo=dlmread('newaveBwmo121.txt','\t','B1..B121')-.4;

%time and date for WMO R values
xrwmo=dlmread('Ravewmo131.txt','\t','A1..A131');
yrwmo=dlmread('Ravewmo131.txt','\t','B1..B131')+.3;

%time and date for WMO V values
xvwmo=dlmread('Vavewmo209.txt','\t','A1..A209');
yvwmo=dlmread('Vavewmo209.txt','\t','B1..B209');

%time array for the fits
t=2455000:.2:2458000;

%shifts in the fits for R
ZR = 13.3406+.3;
%shifts in the fits for V
ZV =13.8644;
%shifts in the fits for B
ZB = 14.5753-.4;

W=dlmread('Rfit.per','\t','A1..A5');
%frequency, amplitude, and phase shift for B
AB=dlmread('Bfit.txt','\t','B1..B5');
PhiB=dlmread('Bfit.txt','\t','C1..C5');
```

```
%frequency, amplitude, and phase shift for R
AR= dlmread('Rfit.per','\t','B1..B5');
PhiR=dlmread('Rfit.per','\t','C1..C5');
%frequency, amplitude, and phase shift for V
AV= dlmread('Vfit.per','\t','B1..B5');
PhiV=dlmread('Vfit.per','\t','C1..C5');

%used to find the fits for different frequencies
%for B
newsumB = AB(1)*sin(2*pi*(W(1)*t+PhiB(1)));
%for R
newsumR= AR(1).*sin(2*pi*(W(1).*t+PhiR(1)));
%for V
newsumV = AV(1).*sin(2*pi*(W(1).*t+PhiV(1)));

%shifts the fits up
yrs = newsumR+ZR;
yvs = newsumV+ZV;
ybs = newsumB+ZB;


plot(xbrovor-2450000, ybrovor,'bx', xrrovor-2450000,yrrovor,'rx',
    xvrovor-2450000,yvrovor,'gx')
hold on
```

```
plot(xbwmo-2450000, ybwmo,'bo', xrwmo-2450000,yrwmo,'ro' ,xvwmo
    -2450000,  yvwmo,'go', t-2450000,...
      yrs, 'r--', t-2450000, yvs, 'g--',t-2450000, ybs, 'b--','
         MarkerSize',10)
axis([5000 8000 13.5 14.4])
xlabel('Julian Date  2450000+ [JD]');
ylabel('Magnitude [mag]')
ax = gca;
ax.XTickMode='manual';
ax=gca;
ax.XTick =5000:500:8000;
whitebg([1,1,1])
legend('ROVOR B','ROVOR R', 'ROVOR V','WMO B','WMO R',...
      'WMO V')
grid minor
set(gca,'YDir','Reverse')

rx = [xrrovor;xrwmo];
ry = [yrrovor; yrwmo];

vx = [xvrovor; xvwmo];
vy = [yvrovor; yvwmo];

bx = [xbrovor; xbwmo];
by = [ybrovor; ybwmo];
```

```

residry=ry;
residvy=vy;
residby=by;

figure
for g = 1:2

    rnewsumres= AR(g+1).*sin(2*pi*(W(g+1).*t+PhiR(g+1)));
    bnewsumres= AB(g+1).*sin(2*pi*(W(g+1).*t+PhiB(g+1)));
    vnewsumres= AV(g+1).*sin(2*pi*(W(g+1).*t+PhiV(g+1)));
    %creating residual
    %--------------------------------------------------------------
    %creating a new vector that will be all of r combined
    %RRRRRRRRRRRRRRR
    %small sum for subtracting to get residuals
    newsumrshort= AR(g).*sin(2*pi*(W(g).*rx+PhiR(g)));
    if g == 1
        residry = residry - newsumrshort-ZR;
    else
        residry = residry - newsumrshort;
    end
    %RRRRRRRRRRRRRRRRRR
    %VVVVVVVVVVVVVVVVVV
    %small sum for subtracting to get residuals
```

```
    newsumvshort= AV(g).*sin(2*pi*(W(g).*vx+PhiV(g)));
    if g == 1
        residvy = residvy- newsumvshort-ZV;
    else
        residvy = residvy - newsumvshort;
    end
    %VVVVVVVVVVVVVVVVVVV
    %BBBBBBBBBBBBBBBBBBBBBBBBBBBBBBBBB

    %small sum for subtracting to get residuals
    newsumbshort= AB(g).*sin(2*pi*(W(g).*bx+PhiB(g)));
    if g == 1
        residby = residby- newsumbshort-ZB;
    else
        residby = residby - newsumbshort;
    end
    %BBBBBBBBBBBBBBBBBBBBBBBBBBBBBBBB

    %writing the residuals to text files
    if g==1
        fileID1 = fopen('data1rx.txt','w');
        fprintf(fileID1,'%6.4f\n' ,rx,residry);
        fclose(fileID1);

        fileID2 = fopen('datarfit1.txt','w');
```

```
        fprintf(fileID2,'%6.4f\n' ,t,rnewsumres);
        fclose(fileID2);

        fileID3 = fopen('data1vx.txt','w');
        fprintf(fileID3,'%6.4f\n' ,vx,residvy);
        fclose(fileID3);

        fileID4 = fopen('datavfit1.txt','w');
        fprintf(fileID4,'%6.4f\n' ,t,vnewsumres);
        fclose(fileID4);

        fileID5 = fopen('data1bx.txt','w');
        fprintf(fileID5,'%6.4f\n' ,bx,residby);
        fclose(fileID5);

        fileID6 = fopen('databfit1.txt','w');
        fprintf(fileID6,'%6.4f\n' ,t,bnewsumres);
        fclose(fileID6);
       %writing the second residuals to text files
    else
        fileID1 = fopen('data2rx.txt','w');
        fprintf(fileID1,'%6.4f\n' ,rx,residry);
        fclose(fileID1);

        fileID2 = fopen('datarfit2.txt','w');
```

```
        fprintf(fileID2,'%6.4f\n' ,t,rnewsumres);
        fclose(fileID2);

        fileID3 = fopen('data2vx.txt','w');
        fprintf(fileID3,'%6.4f\n' ,vx,residvy);
        fclose(fileID3);

        fileID4 = fopen('datavfit2.txt','w');
        fprintf(fileID4,'%6.4f\n' ,t,vnewsumres);
        fclose(fileID4);

        fileID5 = fopen('data2bx.txt','w');
        fprintf(fileID5,'%6.4f\n' ,bx,residby);
        fclose(fileID5);

        fileID6 = fopen('databfit2.txt','w');
        fprintf(fileID6,'%6.4f\n' ,t,bnewsumres);
        fclose(fileID6);
    end
    %used to create the plots of residuals, where g increments to plot the next
    %frequency cycling from R -> V -> B.
    subplot(3,2,g)
    plot(rx-2450000,residry,'r.',t-2450000,rnewsumres,'m--');
    axis([5000 7700 -.1 .1])
```

```
    ylabel('Residual [mag]');%show y axis on left column
    xlabel('Julian Date [JD]'); %show JD only on the bottom graph

    subplot(3,2,g+2)
    plot(vx-2450000,residvy,'g.',t-2450000,vnewsumres,'y-');
    axis([5000 7700 -.1 .1])
    xlabel('Julian Date [JD]'); %show JD only on the bottom graph
    ylabel('Residual [mag]');%show y axis on left column

    subplot(3,2,g+4);
    plot(bx-2450000,residby,'b.',t-2450000,bnewsumres,'c-');
    axis([5000 7700 -.15 .15])
    ylabel('Residual [mag]'); %show y axis on left column
    xlabel('Julian Date [JD]'); %show JD only on the bottom graph
end
```

Appendix E

2010–2016 Light Curve Data

E.1 B Filter Data

Table E.1
ROVOR B Filter Data (5")
B5asrovor.txt

AJD [JD]	Magnitude (mag)				
2455273.85	14.54704	2455418.685	14.54179	2456450.737	14.631578
2455276.031	14.57083304	2455434.689	14.54394	2456457.848	14.615
2455276.99	14.54313	2455442.656	14.58464	2456462.841	14.60520338
2455304.957	14.52674	2455638.981	14.695965	2457133.943	14.57945667
2455305.864	14.518165	2455791.687	14.68699		
2455323.784	14.55985667	2456448.725	14.62176083		

Table E.2
WMO B Filter Data (5")
newaveBwmo121.txt

AJD [JD]	Magnitude (mag)

2456084.856	14.69	2456410.892	14.611	2456422.79	14.6625
2456184.639	14.659	2456414.795	14.6515	2456426.773	14.672
2456427.787	14.647	2456550.629	14.62	2457187.745	14.5115
2456433.783	14.607	2456551.631	14.625	2457195.772	14.483
2456436.873	14.60566667	2456555.673	14.614	2457196.832	14.455
2456446.802	14.603	2456556.617	14.62	2457199.798	14.4425
2456448.794	14.6	2456558.618	14.601	2457200.785	14.441
2456449.793	14.609	2456559.605	14.602	2457215.807	14.51533333
2456452.81	14.6025	2456564.649	14.595	2457219.699	14.5265
2456457.855	14.616	2456566.655	14.605	2457227.817	14.499
2456458.847	14.608	2456570.666	14.58	2457230.681	14.488
2456460.81	14.595	2456571.677	14.571	2457231.697	14.517
2456461.711	14.597	2456584.595	14.511	2457232.687	14.513
2456465.815	14.632	2456585.601	14.5	2457233.683	14.515
2456470.787	14.6555	2456586.593	14.516	2457252.692	14.50866667
2456483.756	14.658	2456587.59	14.5205	2457256.73	14.43066667
2456492.791	14.64966667	2456588.631	14.528	2457257.647	14.415
2456494.762	14.6775	2456589.594	14.456	2457272.633	14.441
2456495.723	14.66466667	2456592.61	14.5305	2457274.624	14.42033333
2456499.751	14.6716	2456598.6	14.534	2457275.623	14.41233333
2456504.727	14.65533333	2456739.939	14.5425	2457276.622	14.40666667
2456508.721	14.66866667	2456808.733	14.43566667	2457277.628	14.419
2456519.69	14.695	2457172.746	14.42533333	2457285.611	14.373
2456520.693	14.64	2457176.769	14.46533333	2457480.938	14.532
2456534.709	14.611	2457177.832	14.47933333	2457485.853	14.471

2456542.65	14.642	2457182.799	14.518	2457512.886	14.539
2456544.725	14.6295	2457186.794	14.518	2457520.826	14.541
2457521.924	14.536	2457563.886	14.488	2457597.732	14.534
2457522.893	14.533	2457565.81	14.471	2457598.74	14.5445
2457527.825	14.546	2457567.821	14.4705	2457609.717	14.563
2457536.779	14.54166667	2457575.838	14.536	2457612.729	14.545
2457537.798	14.54233333	2457576.832	14.535	2457613.734	14.563
2457539.722	14.528	2457577.803	14.5435	2457614.728	14.56566667
2457540.764	14.54	2457578.838	14.545	2457625.786	14.55666667
2457541.76	14.551	2457581.791	14.5485	2457640.631	14.52766667
2457542.775	14.524	2457582.781	14.528	2457641.628	14.53266667
2457543.819	14.527	2457583.783	14.543	2457648.624	14.52066667
2457544.751	14.502	2457584.875	14.5365	2457671.611	14.43866667
2457556.891	14.48	2457586.784	14.527	2457673.591	14.391
2457560.807	14.469	2457596.734	14.544		

E.2 V Filter Data

Table E.3
ROVOR V Filter Data (5”)
V5asrovor.txt

AJD [JD]	Magnitude (mag)				
2455273.854	13.803267	2456450.714	13.85840791	2457227.737	13.823817
2455275.946	13.84774347	2456457.745	13.892597	2457233.705	13.84263367
2455276.999	13.83100033	2456462.839	13.887195	2457276.649	13.78358367
2455304.962	13.785067	2457307.609	13.75578367	2457277.659	13.781367

2455323.876	13.85650729	2457263.657	13.77295033	2457284.645	13.76048367
2455418.687	13.82610033	2457228.734	13.82460033	2457285.639	13.768267
2455434.691	13.823067	2457290.631	13.757617	2457289.635	13.764117
2455440.659	13.845867	2457274.645	13.782617	2457308.605	13.75088367
2455442.657	13.851967	2457133.945	13.895467	2457306.609	13.756967
2455638.983	13.931967	2457273.645	13.79065033	2457481.995	13.856217
2455791.702	13.922967	2457304.609	13.75003367	2457482.21	13.83393367
2456448.701	13.864903	2457226.696	13.828027	2457485.997	13.844717
2457495.973	13.813367	2457583.775	13.86473367	2457512.954	13.839867
2457496.975	13.81328367	2457584.791	13.850167	2457521.903	13.85413367
2457497.974	13.83185033	2457593.741	13.84953367	2457540.894	13.85258367
2457498.982	13.81968367	2457597.729	13.853267	2457598.729	13.84515033
2457575.871	13.84718367	2457541.861	13.83655033	2457647.652	13.825917
2457577.86	13.856417	2457564.844	13.833117		

Table E.4
WMO V Filter Data (5”)
Vavewmo209.txt

AJD [JD]	Magnitude [mag]				
2456084.856	13.94	2456108.849	13.909	2456131.866	13.879
2456088.839	13.94925	2456109.851	13.89675	2456132.734	13.8645
2456090.748	13.9305	2456110.778	13.9025	2456134.767	13.8725
2456091.725	13.9335	2456111.842	13.886	2456142.718	13.8965
2456092.782	13.94325	2456112.712	13.8825	2456144.833	13.8895
2456093.796	13.94075	2456115.72	13.8575	2456146.692	13.888
2456094.817	13.93475	2456116.766	13.859	2456147.688	13.875

2456095.837	13.92625	2456117.74	13.853	2456149.711	13.8815
2456098.865	13.9225	2456118.762	13.87	2456154.697	13.8825
2456099.799	13.9115	2456119.766	13.8755	2456156.668	13.9035
2456102.762	13.9105	2456120.893	13.8745	2456157.682	13.9055
2456103.875	13.916	2456124.767	13.888	2456158.671	13.9105
2456104.953	13.9245	2456125.854	13.874	2456160.673	13.927
2456105.724	13.92	2456126.749	13.8795	2456163.676	13.946
2456106.709	13.915	2456127.747	13.8875	2456164.667	13.9375
2456165.749	13.9355	2456205.624	13.91	2456448.792	13.879
2456166.743	13.9345	2456206.618	13.9145	2456452.812	13.876
2456168.797	13.9325	2456207.632	13.9275	2456457.853	13.8785
2456173.698	13.9085	2456208.597	13.923	2456458.845	13.8905
2456174.673	13.9075	2456209.609	13.918	2456460.814	13.882
2456175.705	13.9225	2456210.606	13.9115	2456461.71	13.8835
2456176.647	13.9235	2456214.69	13.9235	2456465.818	13.904
2456178.659	13.9295	2456215.641	13.931	2456470.784	13.9115
2456179.646	13.929	2456216.607	13.928	2456483.759	13.916
2456180.664	13.9365	2456218.602	13.9285	2456484.828	13.92
2456183.631	13.9355	2456219.607	13.9345	2456492.805	13.928875
2456184.628	13.9135	2456220.632	13.93	2456494.776	13.9265
2456185.641	13.9195	2456221.603	13.9255	2456495.746	13.924625
2456186.647	13.9215	2456235.57	13.90533333	2456499.769	13.9232
2456188.66	13.9185	2456236.627	13.904	2456504.733	13.90675
2456189.635	13.9325	2456239.625	13.89966667	2456508.717	13.91475
2456190.624	13.9315	2456410.885	13.905	2456518.68	13.891

2456191.626	13.9285	2456414.793	13.915	2456519.688	13.8975
2456192.624	13.942	2456422.793	13.925	2456534.713	13.898
2456193.639	13.9275	2456426.777	13.925	2456542.652	13.9155
2456198.651	13.937	2456427.79	13.919	2456544.722	13.8915
2456201.613	13.9285	2456433.786	13.889	2456550.633	13.8925
2456202.615	13.916	2456436.886	13.89533333	2456556.306	13.897
2456203.625	13.9165	2456444.917	13.88625	2456558.621	13.885
2456204.613	13.9085	2456446.8	13.8645	2456564.653	13.8775
2456566.657	13.879	2457199.802	13.791	2457536.733	13.8565
2456570.669	13.867	2457200.788	13.776	2457537.799	13.85633333
2456571.68	13.853	2457215.808	13.82566667	2457539.724	13.856
2456577.68	13.8365	2457219.702	13.84166667	2457540.767	13.855
2456584.598	13.82	2457227.818	13.81933333	2457541.763	13.8585
2456585.608	13.817	2457230.682	13.817	2457542.779	13.8455
2456586.596	13.8155	2457231.698	13.8285	2457543.823	13.847
2456598.602	13.833	2457232.688	13.825	2457544.756	13.834
2456797.82	13.81466667	2457233.685	13.827	2457556.894	13.8165
2456800.848	13.78722222	2457252.693	13.82533333	2457560.814	13.802
2456804.894	13.78745833	2457256.731	13.77666667	2457563.884	13.816
2456808.728	13.766	2457257.651	13.76466667	2457565.81	13.808
2456812.897	13.77234615	2457272.634	13.78366667	2457567.819	13.8075
2456813.889	13.78688636	2457274.625	13.778	2457573.777	13.838
2456818.903	13.81764286	2457275.624	13.77233333	2457575.839	13.8455
2456820.897	13.80618182	2457276.623	13.762	2457576.833	13.8435
2457172.749	13.774	2457277.629	13.772	2457577.804	13.8435

2457174.739	13.77166667	2457285.615	13.756	2457578.839	13.8515
2457175.744	13.78433333	2457480.945	13.84733333	2457581.793	13.8465
2457176.77	13.798	2457481.931	13.8465	2457582.782	13.8435
2457177.834	13.81133333	2457485.854	13.805	2457583.782	13.845
2457182.802	13.82833333	2457512.887	13.8465	2457584.876	13.8435
2457187.744	13.82	2457520.829	13.8515	2457586.785	13.838
2457195.773	13.80833333	2457521.925	13.849	2457596.736	13.845
2457196.837	13.785	2457522.896	13.845	2457597.733	13.839
2457598.742	13.8405	2457614.732	13.86166667	2457646.705	13.836
2457609.72	13.866	2457625.787	13.855	2457648.627	13.8305
2457612.73	13.86	2457640.634	13.84266667	2457671.612	13.783
2457613.734	13.86234545	2457641.629	13.8375	2457673.592	13.749

E.3 R Filter Data

Table E.5
ROVOR R Filter Data (5”)
R5asrovor.txt

AJD [JD]	Magnitude (mag)				
2455272.843	13.31587543	2455791.712	13.36737067	2457263.657	13.272864
2455273.863	13.293804	2456415.974	13.39119966	2457228.734	13.314279
2455275.935	13.332504	2456416.929	13.39158893	2457290.631	13.247924
2455277.004	13.29593734	2456443.892	13.37299567	2457274.645	13.275464
2455304.939	13.22796885	2456445.797	13.36932214	2457133.948	13.362904
2455305.982	13.28679567	2456447.811	13.34473682	2457273.645	13.276304
2455323.878	13.32741092	2456448.832	13.3614736	2457304.609	13.260364

2455418.688	13.292104	2456450.841	13.35708396	2457226.695	13.304944
2455434.693	13.316904	2456454.885	13.33948577	2457227.737	13.309844
2455440.661	13.302304	2456457.85	13.351	2457233.705	13.311524
2455442.659	13.311354	2456462.839	13.370532	2457276.649	13.278864
2455638.985	13.376529	2457307.609	13.261044	2457277.659	13.273944
2457284.645	13.270384	2457496.975	13.312364	2457541.861	13.323124
2457285.639	13.267964	2457485.997	13.314184	2457564.843	13.309164
2457289.635	13.256124	2457498.982	13.304104	2457512.954	13.335524
2457308.605	13.264364	2457575.871	13.323324	2457521.903	13.325524
2457306.609	13.260624	2457577.86	13.327384	2457540.894	13.327304
2457481.995	13.337444	2457583.775	13.340524	2457598.729	13.313404
2457484.987	13.332864	2457583.775	13.312344	2457647.658	13.30198734
2457485.997	13.329544	2457593.741	13.332664		
2457495.973	13.306144	2457597.729	13.317644		

Table E.6
WMO R Filter Data (5")
Ravewmo131.txt

AJD [JD]	Magnitude [mag]				
2456084.856	13.402	2456433.788	13.369	2456470.778	13.3645
2456091.761	13.39525	2456436.905	13.368	2456483.761	13.3835
2456092.838	13.40325	2456444.902	13.36975	2456484.826	13.392
2456093.709	13.39725	2456446.798	13.3365	2456492.781	13.40108333
2456094.906	13.398	2456448.79	13.3535	2456495.71	13.39163636
2456095.75	13.38725	2456449.789	13.353	2456499.729	13.38927273
2456098.759	13.389	2456452.814	13.3515	2456504.732	13.37407692

2456184.642	13.383	2456457.851	13.3555	2456508.715	13.37430769
2456410.888	13.34766667	2456458.842	13.361	2456518.681	13.365
2456422.795	13.3875	2456460.816	13.3555	2456519.687	13.358
2456426.778	13.3885	2456461.708	13.355	2456520.698	13.3685
2456427.793	13.381	2456465.82	13.3775	2456534.717	13.3755
2456542.654	13.3735	2457172.747	13.2618	2457277.63	13.26166667
2456544.72	13.357	2457174.742	13.264	2457285.611	13.2545
2456550.636	13.356	2457175.745	13.26833333	2457481.934	13.335
2456558.624	13.346	2457176.774	13.278	2457485.855	13.296
2456559.611	13.3255	2457177.838	13.291	2457512.889	13.3205
2456564.655	13.338	2457182.801	13.2985	2457520.832	13.324
2456566.659	13.343	2457187.745	13.302	2457521.926	13.324
2456570.672	13.333	2457195.774	13.2895	2457522.897	13.322
2456571.682	13.325	2457196.834	13.268	2457527.829	13.335
2456584.6	13.3065	2457199.804	13.27133333	2457536.762	13.32875
2456585.61	13.304	2457200.791	13.25666667	2457537.8	13.32433333
2456588.635	13.328	2457215.807	13.299	2457539.725	13.324
2456589.599	13.4265	2457219.704	13.318	2457540.769	13.3285
2456598.604	13.312	2457227.819	13.293	2457541.764	13.3215
2456741.912	13.327	2457230.683	13.297	2457542.78	13.322
2456799.779	13.282	2457231.699	13.304	2457543.824	13.327
2456800.799	13.277875	2457232.689	13.29066667	2457544.755	13.3195
2456804.773	13.27488889	2457233.686	13.30066667	2457556.896	13.296
2456808.73	13.26033333	2457252.694	13.29933333	2457560.813	13.283
2456812.776	13.2605	2457256.733	13.265	2457565.811	13.29

2456813.773	13.26644444	2457257.654	13.24733333	2457567.819	13.289
2456814.711	13.27566667	2457272.635	13.272	2457573.778	13.316
2456818.822	13.2885	2457274.626	13.26966667	2457575.84	13.316
2456820.773	13.29116667	2457275.625	13.266	2457576.834	13.32566667
2456821.727	13.294	2457276.624	13.26133333	2457577.805	13.3155
2457578.84	13.32	2457597.732	13.31	2457640.636	13.33
2457581.793	13.317	2457598.742	13.3135	2457641.63	13.32066667
2457582.783	13.3125	2457609.721	13.3315	2457646.706	13.301
2457583.785	13.3085	2457612.731	13.3325	2457648.63	13.29833333
2457584.877	13.309	2457613.735	13.327	2457671.617	13.284
2457586.786	13.3105	2457614.734	13.329	2457673.593	13.265
2457596.737	13.314	2457625.788	13.33166667		

Appendix F

Residuals

Table F.1 Residuals for B

AJD [JD]	1st Res. [mag]	2nd Res. [mag]			
2455273.85	0.004	0.0048	2455442.656	0.0001	-0.0135
2455276.031	0.0273	0.0251	2455638.981	0.0594	0.049
2455276.99	-0.0006	-0.0041	2455791.687	0.0159	-0.0058
2455304.957	-0.0232	-0.0497	2456448.725	-0.0339	-0.0146
2455305.864	-0.032	-0.0584	2456450.737	-0.0237	-0.0063
2455323.784	0.0055	-0.008	2456457.848	-0.0386	-0.0298
2455418.685	-0.0364	-0.0622	2456462.841	-0.0473	-0.0453
2455434.689	-0.0385	-0.0602	2457133.943	0.0729	0.0921
2455440.658	-0.0113	-0.0273	2456084.856	0.0156	0.0402
2456184.639	-0.0116	0.0098	2456519.69	0.0827	0.077
2456410.892	-0.0266	-0.0181	2456520.693	0.0279	0.0237
2456414.795	0.0148	0.0282	2456534.709	0.0024	0.0169
2456422.79	0.0275	0.0491	2456542.65	0.0355	0.0577

2456426.773	0.0378	0.0621	2456544.725	0.0235	0.0472
2456427.787	0.0131	0.0379	2456550.629	0.0155	0.0417
2456433.783	-0.0256	0.0008	2456551.631	0.0208	0.0471
2456436.873	-0.0263	0	2456555.673	0.0108	0.0371
2456446.802	-0.0267	-0.0056	2456556.617	0.0171	0.0432
2456448.794	-0.0293	-0.01	2456558.618	-0.0014	0.0241
2456449.793	-0.0201	-0.0017	2456559.605	-0.0002	0.025
2456452.81	-0.0259	-0.0108	2456564.649	-0.0059	0.0162
2456457.855	-0.0112	-0.0024	2456566.655	0.0047	0.025
2456458.847	-0.019	-0.0115	2456570.666	-0.0193	-0.003
2456460.81	-0.0315	-0.0268	2456571.677	-0.028	-0.0128
2456461.711	-0.0293	-0.0258	2456584.595	-0.0846	-0.0865
2456465.815	0.0066	0.0044	2456585.601	-0.0954	-0.0987
2456470.787	0.0313	0.0223	2456586.593	-0.0791	-0.0838
2456483.756	0.0369	0.0141	2456587.59	-0.0743	-0.0804
2456492.791	0.0307	0.0043	2456588.631	-0.0666	-0.074
2456494.762	0.059	0.0325	2456589.594	-0.1383	-0.147
2456495.723	0.0464	0.02	2456592.61	-0.063	-0.0756
2456499.751	0.0543	0.029	2456598.6	-0.0579	-0.0771
2456504.727	0.0393	0.0169	2456739.939	-0.0115	-0.0357
2456508.721	0.0536	0.0347	2456808.733	-0.1007	-0.0845
2457172.746	-0.0524	-0.045	2457285.611	-0.1041	-0.089
2457176.769	-0.0123	-0.0103	2457480.938	0.0348	0.0421
2457177.832	0.0018	0.0022	2457485.853	-0.0271	-0.0134
2457182.799	0.0407	0.0342	2457512.886	0.0362	0.0606

2457186.794	0.0408	0.0291	2457520.826	0.0367	0.0548
2457187.745	0.0344	0.0215	2457521.924	0.0315	0.0484
2457195.772	0.0061	-0.0151	2457522.893	0.0283	0.0442
2457196.832	-0.0218	-0.0439	2457527.825	0.0404	0.0503
2457199.798	-0.0343	-0.0584	2457536.779	0.0343	0.0319
2457200.785	-0.0357	-0.0604	2457537.798	0.0347	0.031
2457215.807	0.0389	0.0147	2457539.722	0.02	0.0136
2457219.699	0.0501	0.0286	2457540.764	0.0318	0.024
2457227.817	0.0227	0.0096	2457541.76	0.0426	0.0335
2457230.681	0.0117	0.0022	2457542.775	0.0154	0.005
2457231.697	0.0407	0.0326	2457543.819	0.0182	0.0064
2457232.687	0.0368	0.0299	2457544.751	-0.007	-0.0199
2457233.683	0.0388	0.0333	2457556.891	-0.0314	-0.0556
2457252.692	0.0323	0.0513	2457560.807	-0.0432	-0.0691
2457256.73	-0.0457	-0.0233	2457563.886	-0.0249	-0.0513
2457257.647	-0.0614	-0.0383	2457565.81	-0.0423	-0.0687
2457272.633	-0.0357	-0.0102	2457567.821	-0.0432	-0.0694
2457274.624	-0.0564	-0.0318	2457573.776	0.001	-0.0226
2457275.623	-0.0644	-0.0404	2457575.838	0.0206	-0.0016
2457276.622	-0.0701	-0.0467	2457576.832	0.0194	-0.002
2457277.628	-0.0578	-0.0351	2457577.803	0.0277	0.0071
2457578.838	0.0289	0.0094	2457612.729	0.0214	0.043
2457581.791	0.0318	0.0152	2457614.728	0.0416	0.0647
2457582.781	0.0111	-0.0044	2457625.786	0.03	0.0564
2457583.783	0.0259	0.0116	2457640.631	-0.0025	0.0147

2457584.875	0.0191	0.0061	2457641.628	0.0022	0.0184
2457586.784	0.0092	-0.0014	2457646.706	0.0073	0.0174
2457596.734	0.024	0.027	2457648.624	-0.0115	-0.0039
2457597.732	0.0138	0.0182	2457671.611	-0.0991	-0.1203
2457598.74	0.024	0.0298	2457673.591	-0.1473	-0.17
2457609.717	0.0401	0.059			

Table F.2 Residuals for V

AJD [JD]	1st Res. [mag]	2nd Res. [mag]			
2455273.854	-0.0302	-0.0111	2457290.631	-0.0465	-0.0311
2455275.946	0.0139	0.0339	2457274.645	-0.0208	-0.0215
2455276.999	-0.003	0.0174	2457133.945	0.0926	0.0731
2455304.962	-0.0531	-0.0454	2457273.645	-0.0128	-0.0146
2455323.876	0.0154	0.003	2457304.609	-0.0547	-0.0336
2455418.687	-0.0306	-0.0177	2457226.696	0.0258	0.0143
2455434.691	-0.0363	-0.0404	2457227.737	0.0216	0.0091
2455440.659	-0.0145	-0.0248	2457233.705	0.0403	0.0231
2455442.657	-0.0088	-0.021	2457276.649	-0.02	-0.0184
2455638.983	0.039	0.0601	2457277.659	-0.0222	-0.0195
2455791.702	0.01	0.0059	2457284.645	-0.0434	-0.0333
2456448.701	-0.0272	-0.0203	2457285.639	-0.0356	-0.0246
2456450.714	-0.0334	-0.0244	2457289.635	-0.0399	-0.0254
2456457.745	0.0018	0.0172	2457308.605	-0.0541	-0.0333
2456462.839	-0.0028	0.0159	2457306.609	-0.0479	-0.0268
2457307.609	-0.0491	-0.0282	2457481.995	0.0361	0.015

2457263.657	-0.0301	-0.0423	2457482.21	0.0138	-0.0073
2457228.734	0.0223	0.009	2457485.997	0.0241	0.0031
2457495.973	-0.0085	-0.0252	2456098.865	-0.0035	0.0103
2457496.975	-0.0087	-0.0247	2456099.799	-0.0145	0.0001
2457497.974	0.0098	-0.0055	2456102.762	-0.0154	0.0013
2457498.982	-0.0025	-0.017	2456103.875	-0.0099	0.0076
2457575.871	0.0145	0.011	2456104.953	-0.0014	0.0168
2457577.86	0.0234	0.0178	2456105.724	-0.0058	0.0127
2457583.775	0.0309	0.0192	2456106.709	-0.0108	0.0083
2457584.791	0.0162	0.0036	2456108.849	-0.0167	0.0033
2457593.741	0.0142	-0.0048	2456109.851	-0.029	-0.0086
2457597.729	0.0173	-0.0032	2456110.778	-0.0232	-0.0026
2457541.861	0.0087	0.0298	2456111.842	-0.0397	-0.0188
2457564.844	0.002	0.0106	2456112.712	-0.0431	-0.0221
2457512.954	0.0159	0.0156	2456115.72	-0.068	-0.0469
2457521.903	0.029	0.0383	2456116.766	-0.0665	-0.0454
2457540.894	0.0249	0.0459	2456117.74	-0.0725	-0.0515
2457598.729	0.0091	-0.0117	2456118.762	-0.0554	-0.0346
2457647.652	-0.0178	-0.0024	2456119.766	-0.0499	-0.0293
2456084.856	0.0136	0.013	2456120.893	-0.0508	-0.0306
2456088.839	0.023	0.0268	2456124.767	-0.0372	-0.0187
2456090.748	0.0043	0.0101	2456125.854	-0.0511	-0.0333
2456091.725	0.0073	0.0142	2456126.749	-0.0456	-0.0283
2456092.782	0.0171	0.0251	2456127.747	-0.0376	-0.0209
2456093.796	0.0146	0.0236	2456131.866	-0.0459	-0.0324

2456094.817	0.0086	0.0187	2456132.734	-0.0604	-0.0477
2456095.837	0.0001	0.0112	2456134.767	-0.0523	-0.0415
2456142.718	-0.0279	-0.0255	2456186.647	-0.0005	-0.0175
2456144.833	-0.0348	-0.0347	2456188.66	-0.0033	-0.019
2456146.692	-0.0362	-0.0382	2456189.635	0.0107	-0.0042
2456147.688	-0.0492	-0.0523	2456190.624	0.0098	-0.0043
2456149.711	-0.0426	-0.0479	2456191.626	0.0069	-0.0064
2456154.697	-0.0413	-0.0518	2456192.624	0.0204	0.0081
2456156.668	-0.0202	-0.0325	2456193.639	0.006	-0.0054
2456157.682	-0.0182	-0.0314	2456198.651	0.0159	0.0095
2456158.671	-0.0131	-0.0272	2456199.611	0.0104	0.0051
2456160.673	0.0035	-0.0122	2456201.613	0.0076	0.0044
2456163.676	0.0226	0.0049	2456202.615	-0.0049	-0.0069
2456164.667	0.0142	-0.0041	2456203.625	-0.0043	-0.0052
2456165.749	0.0123	-0.0066	2456204.613	-0.0122	-0.012
2456166.743	0.0113	-0.008	2456205.624	-0.0106	-0.0093
2456168.797	0.0094	-0.0107	2456206.618	-0.0061	-0.0036
2456173.698	-0.0143	-0.0354	2456207.632	0.007	0.0106
2456174.673	-0.0152	-0.0364	2456208.597	0.0026	0.0072
2456175.705	-0.0002	-0.0213	2456209.609	-0.0023	0.0034
2456176.647	0.0009	-0.0202	2456210.606	-0.0088	-0.002
2456178.659	0.007	-0.0137	2456214.69	0.0035	0.0145
2456179.646	0.0066	-0.0139	2456215.641	0.0111	0.0229
2456180.664	0.0141	-0.006	2456216.607	0.0082	0.0209
2456183.631	0.0133	-0.0055	2456218.602	0.0088	0.0233

2456184.628	-0.0086	-0.0269	2456219.607	0.0149	0.0301
2456185.641	-0.0025	-0.0202	2456220.632	0.0105	0.0265
2456221.603	0.0061	0.0228	2456495.746	0.0398	0.0466
2456235.57	-0.0129	0.0082	2456499.769	0.0391	0.0414
2456236.627	-0.0142	0.0068	2456504.733	0.0234	0.0202
2456239.625	-0.0182	0.0021	2456508.717	0.0321	0.0246
2456410.885	0.0073	-0.0138	2456518.68	0.0099	-0.0065
2456414.793	0.0178	-0.0032	2456519.688	0.0166	-0.0005
2456422.793	0.029	0.0108	2456520.696	0.0193	0.0015
2456426.777	0.0296	0.014	2456534.713	0.0196	-0.0013
2456427.79	0.0237	0.009	2456542.652	0.0384	0.0207
2456433.786	-0.0054	-0.0147	2456544.722	0.0147	-0.0016
2456436.886	0.0014	-0.0047	2456550.633	0.0167	0.0054
2456444.917	-0.0065	-0.0037	2456556.306	0.0222	0.0166
2456446.8	-0.0279	-0.023	2456558.621	0.0106	0.0075
2456448.792	-0.0131	-0.0061	2456564.653	0.0041	0.0077
2456452.812	-0.0155	-0.0044	2456566.657	0.0059	0.0118
2456457.853	-0.0122	0.0032	2456570.669	-0.0054	0.0046
2456458.845	-0.0001	0.0161	2456571.68	-0.0192	-0.0083
2456460.814	-0.0083	0.0092	2456577.68	-0.0347	-0.0187
2456461.71	-0.0067	0.0114	2456584.598	-0.0501	-0.0301
2456465.818	0.0145	0.0345	2456585.608	-0.0529	-0.0326
2456470.784	0.0228	0.0439	2456586.596	-0.0542	-0.0336
2456483.759	0.0293	0.0466	2456598.602	-0.0347	-0.0151
2456484.828	0.0335	0.0501	2456797.82	-0.0204	-0.0221

2456492.805	0.0436	0.0534	2456800.848	-0.0474	-0.0457
2456494.776	0.0416	0.0493	2456804.894	-0.0465	-0.0404
2456808.728	-0.0674	-0.0573	2457257.651	-0.0382	-0.0552
2456812.897	-0.0605	-0.0466	2457272.634	-0.0197	-0.0227
2456813.889	-0.0458	-0.0311	2457274.625	-0.0255	-0.0262
2456818.903	-0.0143	0.0039	2457275.624	-0.0312	-0.0308
2456820.897	-0.0255	-0.0062	2457276.623	-0.0415	-0.04
2457172.749	-0.0281	-0.0119	2457277.629	-0.0316	-0.0289
2457174.739	-0.0304	-0.0129	2457285.615	-0.0479	-0.0369
2457175.744	-0.0177	0.0004	2457480.945	0.0273	0.0064
2457176.77	-0.0041	0.0146	2457481.931	0.0264	0.0053
2457177.834	0.0093	0.0285	2457485.854	-0.0156	-0.0366
2457182.802	0.0263	0.0472	2457512.887	0.0225	0.0221
2457187.744	0.018	0.0391	2457520.829	0.0265	0.0348
2457195.773	0.0063	0.0248	2457521.925	0.0238	0.0332
2457196.837	-0.017	0.0008	2457522.896	0.0197	0.0301
2457199.802	-0.011	0.0048	2457536.733	0.0294	0.0494
2457200.788	-0.026	-0.0109	2457537.799	0.029	0.0494
2457215.808	0.0236	0.0235	2457539.724	0.0284	0.0493
2457219.702	0.0395	0.0352	2457540.767	0.0273	0.0483
2457227.818	0.0171	0.0045	2457541.763	0.0307	0.0518
2457230.682	0.0147	-0.0003	2457542.779	0.0175	0.0387
2457231.698	0.0262	0.0104	2457543.823	0.0189	0.04
2457232.688	0.0227	0.0062	2457544.756	0.0058	0.0268
2457233.685	0.0247	0.0075	2457556.894	-0.0134	0.0023

2457252.693	0.0226	0.0029	2457560.814	-0.0285	-0.0161
2457256.731	-0.0262	-0.0438	2457563.884	-0.0149	-0.0054
2457565.81	-0.0232	-0.0157	2457597.733	0.0031	-0.0174
2457567.819	-0.024	-0.0186	2457598.742	0.0044	-0.0163
2457573.777	0.0056	0.0044	2457609.72	0.0282	0.0086
2457575.839	0.0128	0.0094	2457612.73	0.0218	0.0036
2457576.833	0.0107	0.0061	2457613.734	0.024	0.0064
2457577.804	0.0105	0.0049	2457614.732	0.0231	0.0063
2457578.839	0.0184	0.0117	2457625.787	0.0147	0.0077
2457581.793	0.0129	0.0032	2457640.634	0.0001	0.0092
2457582.782	0.0098	-0.0009	2457641.629	-0.0053	0.0048
2457583.782	0.0112	-0.0005	2457646.705	-0.0076	0.0071
2457584.876	0.0095	-0.0032	2457648.627	-0.0134	0.0028
2457586.785	0.0037	-0.0106	2457671.612	-0.0646	-0.0461
2457596.736	0.0092	-0.011	2457673.592	-0.0989	-0.0816

Table F.3 Residuals for R

AJD [JD]	1st Res. [mag]	2nd Res. [mag]			
2455272.843	0.0041	0.0152	2456448.832	-0.0048	0.004
2455273.863	-0.0182	-0.0071	2456450.841	-0.0089	0.0006
2455275.935	0.0203	0.0311	2456454.885	-0.026	-0.0154
2455277.004	-0.0164	-0.0057	2456457.85	-0.014	-0.003
2455304.939	-0.0883	-0.0905	2456462.839	0.0062	0.0173
2455305.982	-0.0296	-0.0324	2457307.609	-0.0246	-0.0161
2455323.878	0.0084	-0.002	2457263.657	-0.0111	-0.0115

2455418.688	-0.0413	-0.0404	2457228.734	0.0311	0.0205
2455434.693	-0.019	-0.0267	2457290.631	-0.0369	-0.026
2455440.661	-0.0345	-0.0444	2457274.645	-0.0088	-0.0031
2455442.659	-0.0258	-0.0361	2457133.948	0.0792	0.0728
2455638.985	0.0096	0.0191	2457273.645	-0.0079	-0.0027
2455791.712	-0.018	-0.0258	2457304.609	-0.0251	-0.0156
2456415.974	0.0204	0.0122	2457226.695	0.0218	0.0116
2456416.929	0.0209	0.0131	2457227.737	0.0267	0.0163
2456443.892	0.006	0.0128	2457233.705	0.0283	0.0171
2456445.797	0.0026	0.0102	2457276.649	-0.0055	0.0012
2456447.811	-0.0217	-0.0133	2457277.659	-0.0104	-0.0033
2457284.645	-0.0142	-0.0045	2456084.856	0.0041	0.0099
2457285.639	-0.0167	-0.0067	2456091.761	-0.0025	0.0063
2457289.635	-0.0287	-0.0179	2456092.838	0.0055	0.0147
2457308.605	-0.0213	-0.0132	2456093.709	-0.0004	0.009
2457306.609	-0.0249	-0.0161	2456094.906	0.0003	0.0101
2457481.995	0.0378	0.028	2456095.75	-0.0104	-0.0004
2457484.987	0.0329	0.024	2456098.759	-0.0086	0.0021
2457485.997	0.0295	0.021	2456184.642	-0.0109	-0.016
2457495.973	0.0049	0.0012	2456410.888	-0.0238	-0.0337
2457496.975	0.0111	0.0079	2456422.795	0.0176	0.0126
2457485.997	0.0141	0.0056	2456426.778	0.0191	0.0163
2457498.982	0.0026	0.0005	2456427.793	0.0118	0.0096
2457575.871	0.0121	0.0046	2456433.788	0.0006	0.0019
2457577.86	0.0159	0.0076	2456436.905	0	0.0031

2457583.775	0.0282	0.018
2457583.775	0.0001	-0.0102
2457593.741	0.019	0.0079
2457597.729	0.0034	-0.0072
2457541.861	0.0164	0.0261
2457564.843	-0.0006	-0.0023
2457512.954	0.0323	0.0382
2457521.903	0.0213	0.0308
2457540.894	0.0207	0.0307
2457598.729	-0.0009	-0.0114
2457647.658	-0.0194	-0.0084
2456483.761	0.0222	0.0264
2456484.826	0.0309	0.0345
2456492.781	0.0411	0.0401
2456495.71	0.0321	0.0294
2456499.729	0.0303	0.0254
2456504.732	0.0159	0.0085
2456508.715	0.0167	0.0078
2456518.681	0.0089	-0.0022
2456519.687	0.0021	-0.0091
2456520.698	0.0127	0.0015
2456534.717	0.0219	0.0136
2456542.654	0.0211	0.0165
2456544.72	0.0049	0.0015
2456550.636	0.0048	0.0048

2456444.902	0.0029	0.0101
2456446.798	-0.0301	-0.0221
2456448.79	-0.0128	-0.004
2456449.789	-0.0132	-0.004
2456452.814	-0.0142	-0.0042
2456457.851	-0.0095	0.0015
2456458.842	-0.0039	0.0072
2456460.816	-0.0091	0.0021
2456461.708	-0.0095	0.0017
2456465.82	0.0136	0.0245
2456470.778	0.0013	0.0111
2456741.912	0.0054	-0.0016
2456799.779	-0.0313	-0.025
2456800.799	-0.0353	-0.0285
2456804.773	-0.0377	-0.0293
2456808.73	-0.0517	-0.0419
2456812.776	-0.051	-0.0403
2456813.773	-0.0449	-0.0341
2456814.711	-0.0356	-0.0246
2456818.822	-0.0222	-0.011
2456820.773	-0.0193	-0.0082
2456821.727	-0.0163	-0.0053
2457172.747	-0.0212	-0.0102
2457174.742	-0.019	-0.0079
2457175.745	-0.0147	-0.0035

2456558.624	-0.004	0.0006	2457176.774	-0.005	0.0061
2456559.611	-0.0243	-0.0192	2457177.838	0.008	0.0191
2456564.655	-0.011	-0.0035	2457182.801	0.0155	0.0258
2456566.659	-0.0057	0.0027	2457187.745	0.0191	0.0279
2456570.672	-0.0151	-0.0053	2457195.774	0.0066	0.0118
2456571.682	-0.0229	-0.0129	2457196.834	-0.0149	-0.0103
2456584.6	-0.0394	-0.0285	2457199.804	-0.0116	-0.0086
2456585.61	-0.0418	-0.031	2457200.791	-0.0263	-0.0238
2456588.635	-0.0173	-0.0072	2457215.807	0.016	0.0099
2456589.599	0.0814	0.0912	2457219.704	0.0349	0.0271
2456598.604	-0.0317	-0.0254	2457227.819	0.0098	-0.0006
2457230.683	0.0138	0.0029	2457542.78	0.0151	0.0246
2457231.699	0.0208	0.0098	2457543.824	0.02	0.0291
2457232.689	0.0074	-0.0037	2457544.755	0.0124	0.0212
2457233.686	0.0174	0.0063	2457556.896	-0.0127	-0.0098
2457252.694	0.0157	0.0092	2457560.813	-0.0262	-0.0255
2457256.733	-0.0187	-0.0232	2457565.811	-0.0199	-0.0221
2457257.654	-0.0364	-0.0404	2457567.819	-0.0211	-0.0246
2457272.635	-0.0122	-0.0075	2457573.778	0.0051	-0.0015
2457274.626	-0.0146	-0.0089	2457575.84	0.0048	-0.0027
2457275.625	-0.0183	-0.0121	2457576.834	0.0143	0.0064
2457276.624	-0.023	-0.0163	2457577.805	0.004	-0.0043
2457277.63	-0.0227	-0.0156	2457578.84	0.0084	-0.0003
2457285.611	-0.0302	-0.0201	2457581.793	0.005	-0.0047
2457481.934	0.0354	0.0255	2457582.783	0.0004	-0.0096

2457485.855	-0.004	-0.0126	2457583.785	-0.0038	-0.014
2457512.889	0.0173	0.0232	2457584.877	-0.0034	-0.0139
2457520.832	0.0199	0.0291	2457586.786	-0.0022	-0.013
2457521.926	0.0197	0.0293	2457596.737	-0.0001	-0.0108
2457522.897	0.0176	0.0275	2457597.732	-0.0042	-0.0148
2457527.829	0.03	0.0409	2457598.742	-0.0009	-0.0113
2457536.762	0.0226	0.0335	2457609.721	0.0156	0.0091
2457537.8	0.0181	0.0288	2457612.731	0.0162	0.0112
2457539.725	0.0175	0.0278	2457613.735	0.0105	0.0061
2457540.769	0.0219	0.0319	2457614.734	0.0124	0.0085
2457541.764	0.0148	0.0245	2457625.788	0.0135	0.016
2457640.636	0.0096	0.0191	2457648.63	-0.0232	-0.0121
2457641.63	0.0002	0.0099	2457671.617	-0.041	-0.0357
2457646.706	-0.0203	-0.0094	2457673.593	-0.0603	-0.0561

Bibliography

Acciari, V. A., et al. 2011, The Astrophysical Journal, 729, 2

Aleksić, J., et al. 2015, Astronomy and Astrophysics, 573, A50

Catanese, M., et al. 1997, ApJ, 487, L143

Chakraborty, N., Cologna, G., Kastendieck, M. A., Rieger, F., Romoli, C., Wagner, S. J., Jacholkowska, A., & Taylor, A. 2016, PoS, ICRC2015, 872

Cologna, G., et al. 2016, PoS, ICRC2015, 761

Holden, M. Brigham Young University, Provo, U.T., 2016, Senior thesis

Kondo, Y., et al. 1981, The Astrophysical Journal, 243

Lynden-Bell, D. 1969, Nature, 223, 690

Moody, J. W., et al. 2012, Publications of the Astronomical Society of the Pacific, 124, 956

Neronov, A., Semikoz, D., & Taylor, A. M. 2012, Astronomy and Astrophysics, 541, A31

Noda, K., Furniss, A., González, J. B., Madejski, G., & Paneque, D. 2015, PoS, ICRC2015, 755

Pace, C. J., Iii, R. L. P., Moody, J. W., Joner, M. D., & Little, B. 2013, Publications of the Astronomical Society of the Pacific, 125, 344

Rivest, L. Brigham Young University, Provo, U.T., 2017, Senior thesis

Urry, C. M., & Padovani, P. 1995, PASP, 107, 803

Index